Electronic Supplementary Material (ESI) for Chemical Communications.

Teaching Photosensitizers a New Trick: Red Light-Triggered G-Quadruplex Alkylation by Ligand Co-localization

Enrico Cadoni‡, Alex Manicardi‡, Mathieu Fosséprè†, Kaat Heirwegh‡, Mathieu Surin†*, Annemieke Madder‡*

‡Organic and Biomimetic Research Group, Faculty of Sciences, Campus Sterre, Krijgslaan 281, Building S4, Gent, Belgium

†Laboratory for Chemistry of Novel Materials, Center of Innovation and Research in Materials and Polymers, University of Mons, Mons, Belgium

Table of contents

1. General

All reagents were purchased from Sigma-Aldrich, Fluka, Merck, TCI Europe, Fluorochem and used without further purification. Dry DMF was stored over 4 Å molecular sieves. TLCs were run on Merck silica 60 on aluminum sheets. Column chromatography was performed as flash chromatography on Grace silica 60 (0.060-0.200 mm). DNA sequences were purchased from IDT (Leuven, Belgium) and are depicted in **Table S1** and **Table S2**.

NMR spectra were recorded on a Brucker Avance 300 or 400. δ values are expressed in ppm relatively either to $CDCl_3$ (7.29 ppm for proton and 76.9 ppm for carbon) or DMSO-d^6 (2.50 ppm for proton and 39.5 ppm for carbon). The following abbreviations are used to explain the multiplicities: s=singlet, d=doublet, t=triplet, q=quartet, m=multiplet, and br=broad.

HPLC-MS data were collected on an Agilent 1100 Series instrument equipped with a Phenomenex Kinetex C18 100 Å column (150 x 4.6 mm, 5 µm at 35°C) connected to an ESMSD type VL mass detector (quadrupole ion trap mass spectrometer) with a flow rate of 1.5 ml/min was used with the following solvent system: (A): 0.1% HCOOH in H_2O and (B) MeCN. Gradient: 100% A for 2 min, then a gradient from 0 to 100% B over 6 min was used, followed by 2 min of flushing with 100% B (HPLC-1).

HPLC-UV data were collected on an Agilent 1100 Series instrument equipped with a Waters X-Bridge BEH C18 XP Column (130Å, 2.5 µm, 4.6 mm X 50 mm) connected to a DAD using a flow rate of 0.80 ml/min with the following solvent system: (A) 0.1 M TEAA-buffer + 5% MeCN and (B) MeCN. Column was flushed for 4 minutes with (A), then a gradient from 0 to 100% B in 12 minutes was used, followed by 4 minutes flush of 100% B, and 4 minutes flush of 100% A (HPLC-2);
For furan-oxidation kinetics of **PDC-A** HPLC was equipped with a Waters XTERRA RP18 5µm column (250 x 2.1 mm at 40°C or 50°C) connected to a DAD using a flow rate of 0.35 ml/min with the following solvent system: (A): 0.1% TFA in H_2O and (B) 0.1% TFA in MeCN. Gradient: 100% A for 1 min, then a gradient from 0 to 10% B in 1 min, then to 30% B in 10 min, and finally to 100% B in 1 min, followed by 3.5 min of flushing with 100% B (HPLC-3).
Purification of final **TAP** ligands was performed in a Gilson PLC-2250, equipped with a Waters C18 15 µm column (300 x 50 mm) using a flow rate of 65 ml/min. The gradient and solvent system used was adapted according to literature.[1]

UV-VIS spectra were recorded using a Trinean DropSense96 UV/VIS droplet reader.

Thermal denaturation experiments were recorded on a Varian Cary 300 Bio instrument equipped with a six-cell thermostatted cell holder.

MALDI-TOF analysis was performed using an Applied Biosystems - 4800 Plus MALDI TOF/TOF™ Analyzer. As matrix, 100mg/ml 2,5-Dihydroxybenzoic acid (DHB) in mQ water : MeCN (1:2) + 0.1% TFA was used.

Alkylation experiments were performed using Eppendorf Thermomixer Comfort for temperature control and Euromex Illuminator EK-1 lamps, equipped with a 100 W halogen lamp LE.5210 and connected to an Euromex LE.5214 dual arm light conductor. Depending on the photosensitizer used for the experiment, an adeguate filter (Euromex LE.5223) was used (red-light filter for MB, green-light filter for RB). Prior each experiment, power of the lamps was measured using a TES 1335 light meter equipped with a custom fitting for the dual-arms. The calculated light power is 0.73 W for the red light and 1.4 W for the green-light, derived from the luminescence value obtained with the light-meter using the equation:

$$P_{(W)} = \frac{E_{(lx)} \times A_{m^2}}{\eta_{(lm/W)}} \qquad (1)$$

Where $P_{(W)}$ is the power expressed in Watts, $E_{(lx)}$ is the illuminance value in lux, A_{m^2} is the detector surface expressed in square meters, and $\eta_{(lm/W)}$ is luminous efficiency of the halogen lamps used (16 lm/W).

2. Ligand synthesis

TAP-A (*N*,*N*'-((4-(furan-2-yl)pyridine-2,6-diyl)bis(4,1-phenylene))bis(3-(pyrrolidin-1-yl)propanamide)), and **PDC-Cl** (4-chloro-N^2,N^6-di(quinolin-3-yl)pyridine-2,6-dicarboxamide) were synthesized as previously reported.[S1,2]

2.1. Triarylpyridines (TAPs)

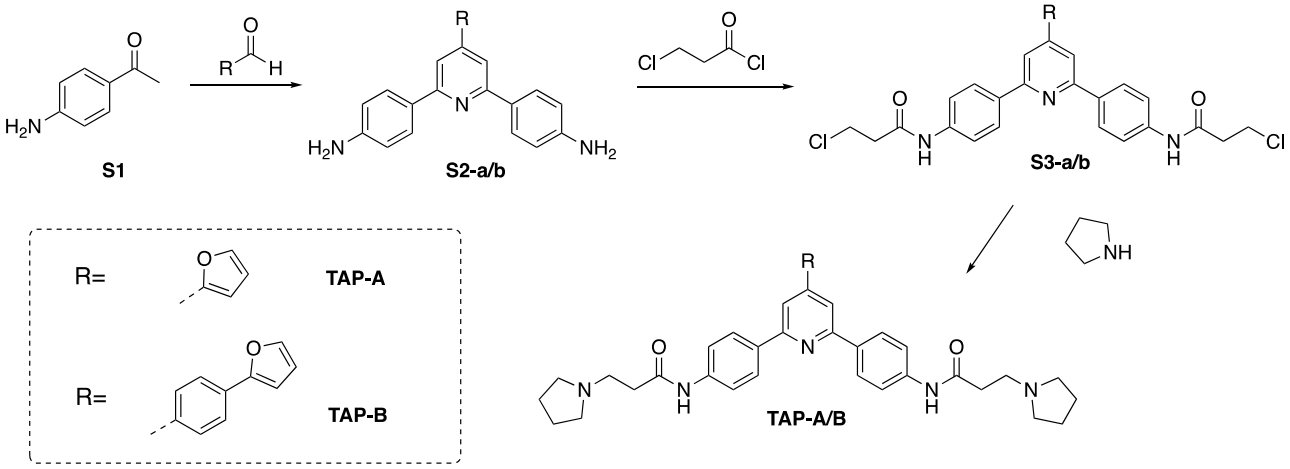

Scheme S1. Synthesis of TAP-based ligands.

4,4'-(4-(4-(furan-2-yl)phenyl)pyridine-2,6-diyl)dianiline [S2-b]

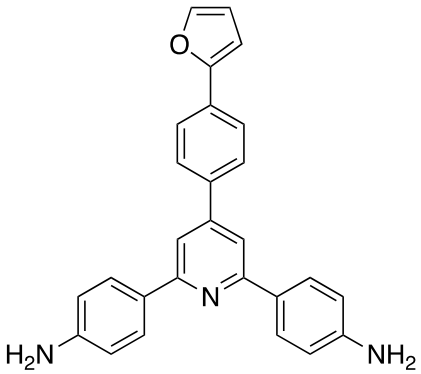

In a round-bottomed flask, p-aminoacetophenone (1.405 g, 2.0 eq., 10.4 mmol) was added to a crushed suspension of NaOH (415.9 mg, 2.0 eq., 10.4 mmol) in PEG-300 (9 mL). The mixture was then heated to 80°C and 4-furyl-benzaldehyde (1.0 eq., 5.2 mmol) was added. Upon addition, the reaction temperature was raised to 110 °C and allowed to react for 3h. Ammonium acetate (6.01 g, 15.0 eq., 78 mmol) was added and the temperature lowered to 100°C, keeping the mixture stirring for 3 additional hours. The solution was then cooled down to room temperature and water (90 mL) added to induce precipitation. The precipitate was collected on Buchner filter, re-suspended in a EtOH:H_2O solution (1:10, 100 mL) and triturated for 25 minutes. The mixture was filtered again and dried overnight under vacuum to give compound **S2-b** as a light brown powder (1.57 g, 74.7%). The product was employed without further purification for the next step after H-NMR and MS analysis **^{1}H-NMR** (400 MHz, Acetone-d_6) δ 8.11 – 8.07 (m, 4H), 8.00 – 7.97 (m, 2H), 7.90 – 7.87 (m, 2H), 7.86 (s, 2H), 7.69 (dd, *J* = 1.8, 0.7 Hz, 1H), 6.97 (dd, *J* = 3.2, 0.6 Hz, 1H), 6.81 – 6.78 (m, 4H), 6.60 (dd, *J* = 3.4, 1.9 Hz, 1H). **LC-MS (ESI, Acetone, rt = 6.91 min)** for $C_{27}H_{21}N_3O$: calc: 403.5, found: 404.1 $[M+H]^+$

N,N'-((4-(4-(furan-2-yl)phenyl)pyridine-2,6-diyl)bis(4,1-phenylene))bis(3-chloropropanamide) [S3-b]

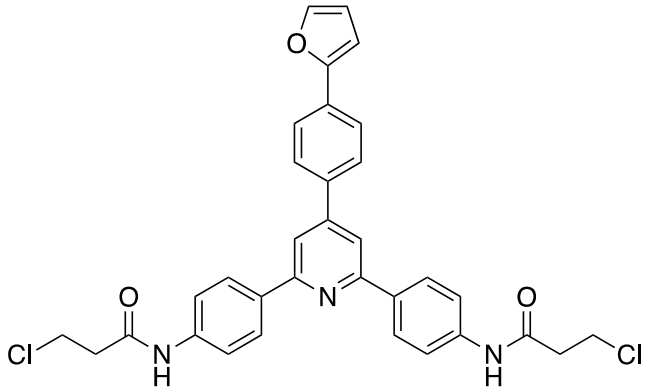

In a round-bottomed flask, 3-chloropropionylchloride (1.8 mL, 27 eq., 16.5 mmol) was slowly added to **S2-b** (250 mg, 1 eq., 0.61 mmol) and the obtained dark mixture was stirred overnight at 60°C. The solution was then cooled with an ice-bath and 20 mL of diethyl ether were added to induce precipitation of the target compound. The precipitate was collected over Buchner filter and washed with diethyl ether. The precipitate was suspended in the minimum volume of methanol, and the solution was centrifuged. The supernatant was evaporated, obtaining a brown oil. **S3-b** was obtained as dark brown powder after precipitation with acetone and filtration over Buchner filter (247.4 mg, 69.4%). **^{1}H-NMR** (400 MHz, methanol-d^{4}) δ 8.29 (s, 2H), 8.10 – 8.03 (m, 2H), 7.98 – 7.92 (m, 4H), 7.89 – 7.81 (m, 6H), 7.57 (dd, J = 1.8, 0.7 Hz, 1H), 6.91 (dd, J = 3.4, 0.7 Hz, 1H), 6.50 (dd, J = 3.5, 1.8 Hz, 1H), 3.81 (t, J = 6.3 Hz, 4H), 2.83 (t, J = 6.3 Hz, 4H). **^{13}C-NMR** (101 MHz, methanol-d^{4}) δ 169.7 156.7, 153.1, 152.4, 143.4, 142.2, 134.0, 133.1, 129.4, 128.5, 126.7, 124.1, 112.0, 119.7, 111.8, 107.3, 39.3, 39.2. **LC-MS (ESI, MeOH, rt = 7.18 min)** for $C_{33}H_{27}Cl_2N_3O_3$: calcd: 583.1 Found: 584.0 $[M+H]^+$.

N,N'-((4-(4-(furan-2-yl)phenyl)pyridine-2,6-diyl)bis(4,1-phenylene))bis(3-(pyrrolidin-1-yl)propanamide) [TAP-B]

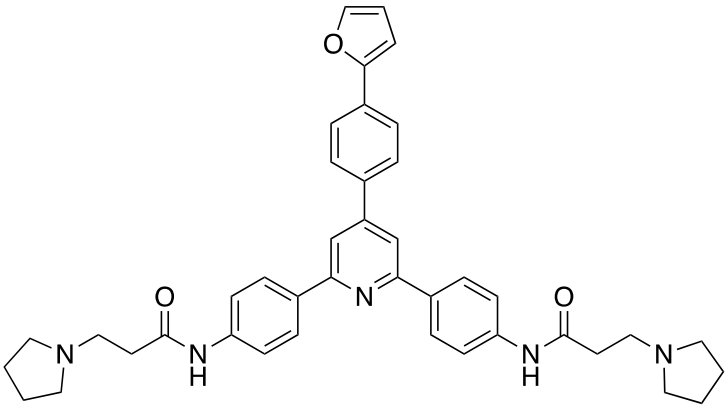

In a screw-cap test tube, compound **S3-b** (25 mg, 1 eq., 0.043 mmol) was dissolved in pyrrolidine (459.8 µL, 130 eq., 5.560 mmol). The mixture obtained was stirred overnight at room temperature. The mixture was then cooled in an ice-bath and ice-cold saturated bicarbonate solution was added to afford a brown precipitate. The mixture was centrifugated and the supernatant was removed. The resulting precipitate was washed twice in MeOH. The merged supernatants were tried under reduced pressure, re-dissolved in 1 mL acetonitrile and TFA and purified by preparative RP-HPLC (*vide supra*) to obtain **TAP-B** (17.1 mg, 60.8%).**^{1}H-NMR** (500 MHz, DMSO-d_6) δ 10.38 (s, 2H), 8.34 – 8.26 (m, 4H), 8.13 (s, 2H), 8.11 – 8.05 (m, 2H), 7.85 (d, *J* = 8.3 Hz, 2H), 7.80 (d, *J* = 1.8 Hz, 1H), 7.78 – 7.72 (m, 4H), 7.10 (d, *J* = 3.4 Hz, 1H), 6.63 (dd, *J* = 3.4, 1.8 Hz, 1H), 3.56 – 3.51 (m, 5H), 3.46 – 3.44 (m, 4H)*, 3.05 (q, *J* = 8.8, 7.8 Hz, 4H), 2.84 (t, *J* = 7.1 Hz, 4H), 2.02 – 1.97 (m, 4H), 1.88 – 1.83 (m, 4H). **^{13}C-NMR** (101 MHz, DMSO-d_6) δ 168.52, 158.77, 158.59, 156.38, 152.94, 140.31, 134.24, 128.29, 127.98, 124.39, 119.58, 118.46, 116.75, 115.62, 112.83, 107.48, 54.05, 50.44, 40.32, 32.61, 23.11. **LC-MS (ESI, DMF, rt= 3.63)** for $C_{41}H_{43}N_5O_3$: calcd: 653.8 Found: 327.2 $[M+2H]^{2+}$

* Partially overlapped with water peak.

2.2. Pyridin-2,6-dicarboxamides (PDCs)

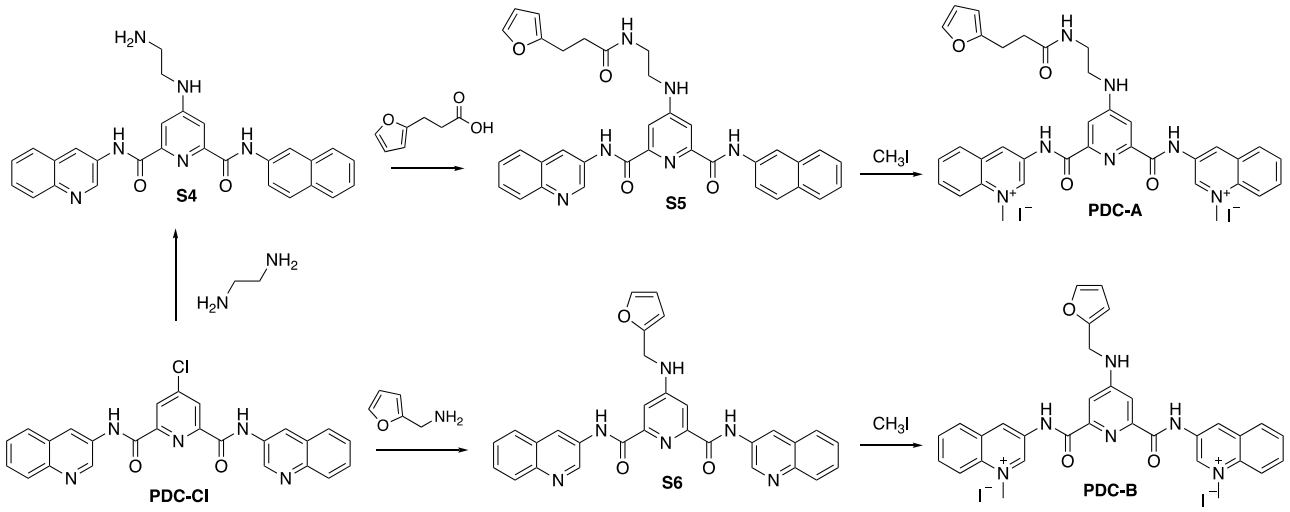

Scheme S2. Synthesis of PDC-based ligands.

4-((2-aminoethyl)amino)-N2,N6-di(quinolin-3-yl)pyridine-2,6-dicarboxamide [S4]

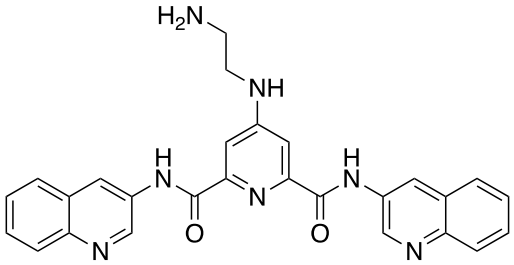

In a test tube with a screw cap, **PDC-Cl** (150 mg, 1 eq., 0.330 mmol) was suspended in 0.5 mL of DMSO, and the mixture was heated to 100°C. Triethylamine (45,94 µL, 1.0 eq, 0.330 mmol) was added to the mixture, followed by the addition of ethylenediamine (353.1 µL, 16 eq, 5.29 mmol). The reaction mixture was then heated to 90°C and stirred overnight. The resulting clear orange solution was then cooled down in an ice-bath and quenched with water (5 mL). The resulting precipitate was filtered over Buchner filter, washed with water and dried under vacuum to afford **S4** as a white powder (138 mg, 87.5%).**^{1}H-NMR** (400 MHz, DMSO-d_6) δ 11.29 (s, 2H), 9.36 (d, J = 2.5 Hz, 2H), 8.96 (d, J = 2.5 Hz, 2H), 8.04 (dt, J = 8.0, 1.6 Hz, 4H), 7.72 (ddd, J = 8.3, 6.8, 1.6 Hz, 2H), 7.67 – 7.54 (m, 4H), 7.50 (t, J = 5.6 Hz, 1H), 3.31 – 3.21 (m, 4H), 2.80 (t, *J* = 6.4 Hz, 2H). **^{13}C-NMR** (101 MHz, DMSO-d_6) δ 163.1, 156.5, 146.1, 144.6, 132.0, 128.7, 128.3, 127.9, 127.8, 127.7, 127.7, 127.1, 124.1, 45.6, 40.5. **LC-MS (ESI, DMF, rt = 5.15 min)**for: $C_{27}H_{23}N_7O_2$ calcd: 477.5 Found: 478.1 $[M+H]^+$.

4-((2-(3-(furan-2-yl)propanamido)ethyl)amino)-N2,N6-di(quinolin-3-yl)pyridine-2,6-dicarboxamide [S5]

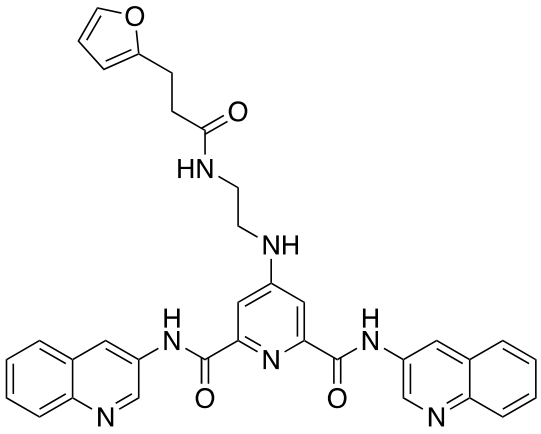

In a round-bottom flask, 2-furylproprionic acid (44.0 mg, 1.5 eq., 0.314 mmol), EDC·Cl (100.4 mg, 2.5 eq., 0.524 mmol) and HOBt (22.1 mg, 0.78 eq., 0.163 mmol) were solubilized in 3 mL dry DMF. **S4** (100 mg, 1 eq., 0,209 mmol) was then added and the reaction mixture was left stirring overnight at room temperature. The reaction mixture was placed on an ice-bath, and water (9 mL) was then added, to afford the formation of a white precipitate. The precipitate was filtered on a Buchner filter, and carefully washed with cold water to afford **S5** as beige powder (110 mg, 87.6%). **^{1}H-NMR** (400 MHz, DMSO-d^6) δ 11.32 (s, 2H), 9.36 (d, *J* = 2.5 Hz, 2H), 8.96 (d, *J* = 2.5 Hz, 2H), 8.17 – 8.07 (m, 1H), 8.04 (dt, *J* = 8.2, 1.7 Hz, 4H), 7.72 (ddd, *J* = 8.3, 6.8, 1.6 Hz, 2H), 7.69 – 7.58 (m, 4H), 7.58 – 7.45 (m, 2H), 6.32 (ddd, *J* = 9.2, 3.2, 1.9 Hz, 1H), 6.08 (dd, *J* = 7.5, 3.1 Hz, 1H), 2.92 – 2.75 (m, 4H), 2.42 (dd, *J* = 8.6, 6.7 Hz, 2H), 1.06 (t, *J* = 7.2 Hz, 2H). **^{13}C-NMR** (101 MHz, DMSO-d_6) δ 171.2, 163.1, 156.4, 154.7, 148.9, 146.1, 144.6, 141.3, 132.0, 128.7, 128.3, 127.9, 127.7, 127.1, 124.1, 110.3, 105.1, 105.0, 45.7, 41.4, 33.6, 23.4. **LC-MS (ESI, DMF)** for: $C_{35}H_{30}N_6O_4$ calcd: 598.7 Found: 599.1 $[M+H]^+$.

3,3'-((4-((2-(3-(furan-2-yl)propanamido)ethyl)amino)pyridine-2,6-dicarbonyl)bis(azanediyl))bis(1-methylquinolin-1-ium) Iodide [PDC-A]

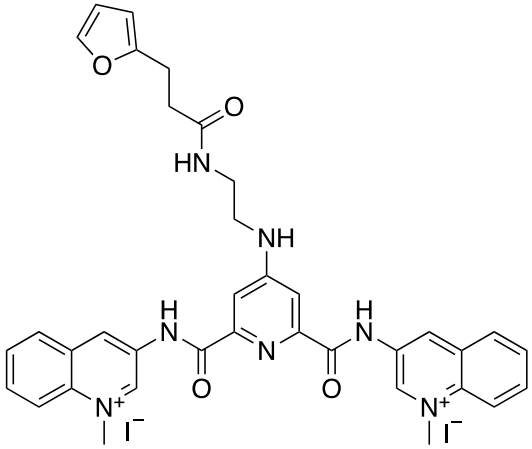

In a screw-cap test tube, **S5** (50 mg, 1 eq., 0.083 mmol) was dissolved in dry DMF. The tube was flushed with argon and methyl iodide (866.9 µL, 167 eq., 13.924 mmol) was added to the reaction mixture and left to stir overnight at room temperature. The reaction was then diluted with diethyl ether (7 mL) and the resulting yellow precipitate was filtered over Buchner filter. The precipitate was washed with Et_2O and dried, to obtain **PDC-A** as a pale-yellow powder (69.6 mg, 94.9%). **^{1}H-NMR** (400 MHz, DMSO-d_6) δ 11.72 (s, 2H), 10.12 (d, J = 2.3 Hz, 2H), 9.65 (d, J = 2.2 Hz, 2H), 8.60 – 8.53 (m, 4H), 8.25 (ddd, J = 8.8, 7.1, 1.2 Hz, 2H), 8.16 – 8.05 (m, 3H), 7.74 (t, J = 5.7 Hz, 1H), 7.64 (s, 2H), 7.48 (d, J = 1.8 Hz, 1H), 6.32 (dd, J = 2.9, 1.9 Hz, 1H), 6.07 (dd, J = 3.3, 0.8 Hz, 1H), 4.79 (s, 6H), 2.85 (t, J = 7.6 Hz, 2H), 2.56 (t, J = 5.5 Hz, 4H), 2.43 (t, J = 7.7 Hz, 2H). **^{13}C-NMR** (101 MHz, DMSO-d_6) δ 206.5, 171.3, 163.1, 156.7, 154.6, 144.7, 141.3, 135.7, 134.2, 134.1, 133.9, 132.4, 130.3, 129.9, 129.2, 119.2, 110.3, 105.0, 46.2, 34.4, 33.5, 30.7, 23.4. **LC-MS (ESI, DMF + 0.1% DMSO, rt= 4.58 min)** for $C_{36}H_{35}N_7O_4$: Calcd: 629,7. Found: 630.1 $[M+H]^+$,314.7 $[M+2H]^{2+}$.

4-((furan-2-ylmethyl)amino)-*N*^{2},*N*^{6}-di(quinolin-3-yl)pyridine-2,6-dicarboxamide [S6]

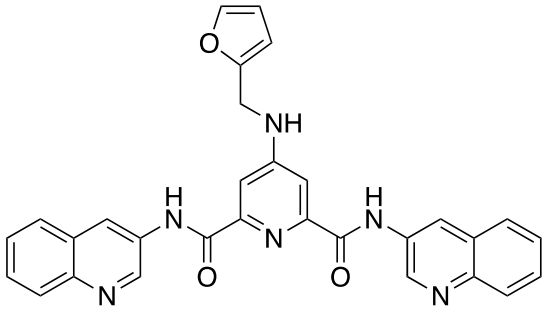

In a sealed test tube, **PDC-Cl** (100 mg, 0.220 mmol, 1.0 eq.) was suspended in furfuryl-amine (2.49 mL, 55.08 mmol, 125 eq.) and TEA (208.5 µL, 0.220 mmol, 1.0 eq) was added to the reaction mixture. The tube was

flushed with argon and the reaction mixture stirred overnight at 90°C. The reaction wash quenched with saturated $NaHCO_3$ solution (9 mL), and the precipitate collected by centrifugation. The precipitate was washed with water and dried. **S6** was re-precipitate with water from acetone and filtered over Buchner filter, obtaining a light brown powder (106 mg, 93.5%). **^{1}H-NMR** (400 MHz, acetone-d_6) δ 9.23 (d, *J* = 2.0 Hz, 2H), 8.90 (d, *J* = 2.0 Hz, 2H), 7.91 (d, *J* = 8.2 Hz, 2H), 7.84 (dd, *J* = 8.2, 1.0 Hz, 2H), 7.67 (s, 2H), 7.55 (ddd, *J* = 8.4, 6.9, 1.5 Hz, 2H), 7.47 (ddd, *J* = 8.1, 6.9, 1.2 Hz, 2H), 7.41 (dd, *J* = 1.8, 0.8 Hz, 1H), 6.32 (d, *J* = 3.2 Hz, 1H), 6.29 (dd, *J* = 3.2, 1.9 Hz, 1H), 4.53 (d, *J* = 4.1 Hz, 2H); **^{13}C-NMR** (101 MHz, acetone-d_6) δ 163.6, 157.3, 152.4, 150.4, 146.4, 146.3, 146.2, 143.5, 133.1, 130.0, 129.1, 128.8, 128.7, 127.9, 123.9, 111.3, 108.6, 40.3; **LC-MS (ESI, DMF, rt = 6.40 min)** for $C_{30}H_{22}N_6O_3$: calcd.: 514.5. Found: 515.7 $[M+H]^+$.

3,3'-((4-((furan-2-ylmethyl)amino)pyridine-2,6-dicarbonyl)bis(azanediyl))bis(1-methylquinolin-1-ium) iodide [PDC-B]

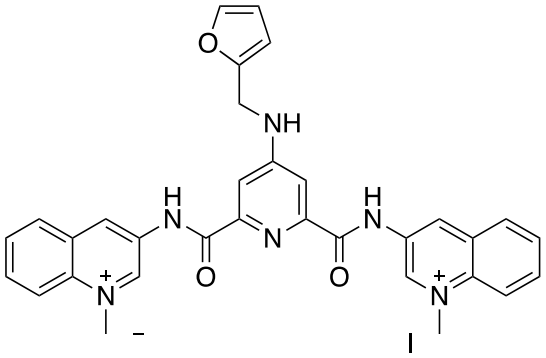

In a sealed test tube, **S6**(40 mg, 0.0777 mmol, 1.0 eq.) was solubilized in DMF (1.2 mL) and flushed with argon. Methyl iodide (0.4 mL, 110 eq) was added dropwise, the tube flushed again with argon, sealed and the mixture was stirred overnight at 40°C. The reaction mixture was poured in Et_2O and the resulting precipitate was filtered over Buchner and washed with Et_2O to afford **PDC-B** as grey powder (51.5 mg, 83.0%). **^{1}H-NMR** (400 MHz, DMSO-d_6) δ 11.73 (s, 2H), 10.13 (d, *J* = 1.8 Hz, 2H), 9.69 – 9.59 (m, 2H), 8.60 – 8.52 (m, 4H), 8.24 (ddd, *J* = 8.8, 7.1, 1.2 Hz, 2H), 8.18 (t, *J* = 5.7 Hz, 1H), 8.13 – 8.06 (m, 2H), 7.72 (s, 2H), 7.67 (dd, *J* = 1.8, 0.8 Hz, 1H), 6.47 (dd, *J* = 3.2, 1.9 Hz, 1H), 6.45 – 6.42 (m, 1H), 4.79 (s, 6H), 4.58 (d, *J* = 5.6 Hz, 2H); **^{13}C-NMR** (101 MHz, DMSO-d_6) δ 163.0, 156.4, 151.1, 144.7, 135.7, 135.2, 134.2, 134.2, 133.9, 132.4, 132.3, 130.3, 129.8, 129.2, 119.2, 110.6, 107.8, 46.1, 39.8 **;**LC-MS(ESI, DMF + 0.1% DMSO, rt= 6.55 min)** for $C_{32}H_{28}N_6O_3^{2+}$: calcd.: 544.6. Found: 544.9 $[M+H]^+$, 272.1 $[M+2H]^{2+}$.

** signal overlaps with DMSO

3. ABDA oxidation experiments

$^1O_2$ production studies were performed monitoring the degradation of 9,10-Anthracenediyl-bis(methylene)dimalonic-acid (ABDA), following the disappearance of its characteristic absorption at 380 nm.[S3]

In a typical experiment a 100 μM working solution of PS was freshly prepared from a 1 mM stock solution and a 200 μM ABDA working solution was freshly prepared from a 500 μM stock solution.
In a 1.5 mL Eppendorf tube, 300 μL of air saturated buffered solution (Tris HCl 100mM, pH 7.4, 10 mM K^+) containing 100 μM ABDA, 1 μM PS and, when required, 5 μM DNA, was prepared. The lamp with the appropriate filter was placed on top of the Eppendorf tube for the entire duration of the experiment. 20 μL samples of solution were collected at different irradiation times and protected from light. Absorbance at 380 nm was recorded via UV-spectroscopy. The PS absorbance at 380 nm wavelength by the two PS, prior and after irradiation, was checked in order to exclude any contribution (figure S1).

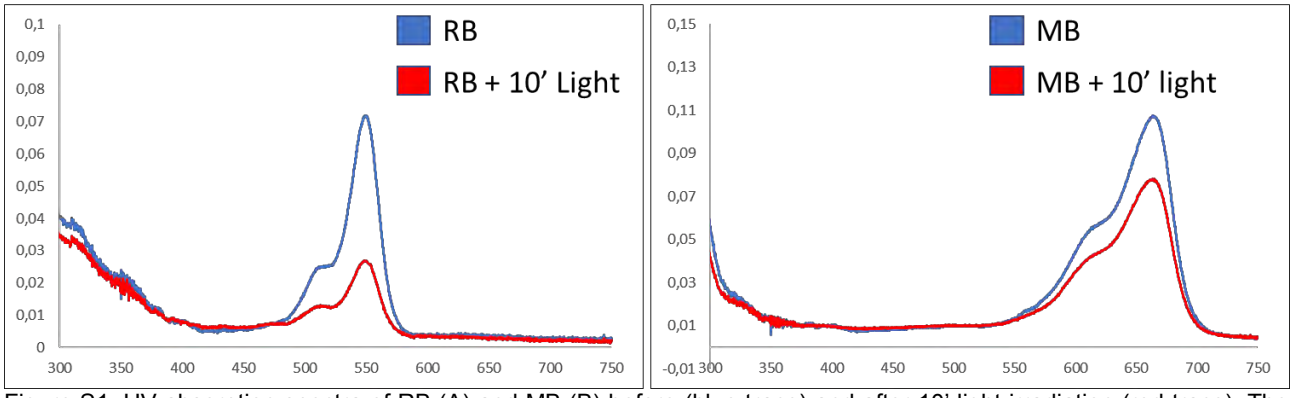

Figure S1. UV absorption spectra of RB (A) and MB (B) before (blue trace) and after 10' light irradiation (red trace). The experiment was performed at a PS concentration of 1 μM, in buffered solution pH 7.4, 10 mM K^+, at 25°C.

In order to check eventual binding of the PS to G4-DNA, a UV-vis analysis was performed, maintaining the same experimental conditions used in the ABDA experiment. As shown in figure S2, the RB absorption profile is not influenced by the presence of G4-DNA, while MB absorption spectra is characterized by a combination of hypochromic effect and bathochromic shift, thus supporting an interaction with the DNA.

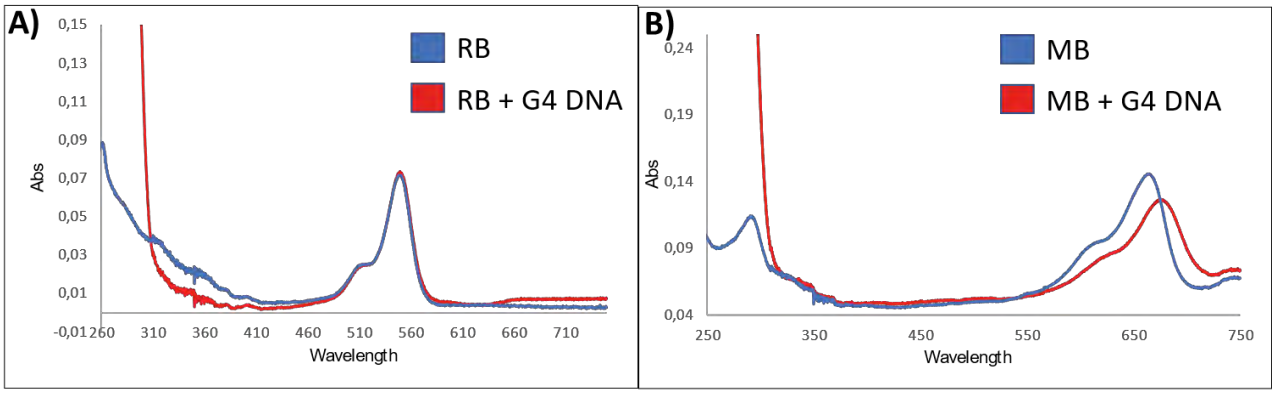

Figure S2. UV absorption spectra of RB (A) and MB (B) in presence (red trace) or absence (blue trace) of DNA-G4. The experiment was performed at ABDA concentration 100 μM, PS concentration 1 μM, in buffered solution pH 7.4, 10 mM K^+, at 25°C.

Additionally, we studied eventual interactions between the PSs and ABDA through UV-Vis spectroscopy., Upon addition of increasing amount of ABDA to a MB solution, a hypochromic effect was observed (Figure S3A), thus supporting the presence of π-π interactions between the two molecules. In contrast, no influence on the RB absorption spectrum was noticed in presence of ABDA up to 100 μM, thus supporting the absence of any interaction between ABDA and RB (Figure S3B).

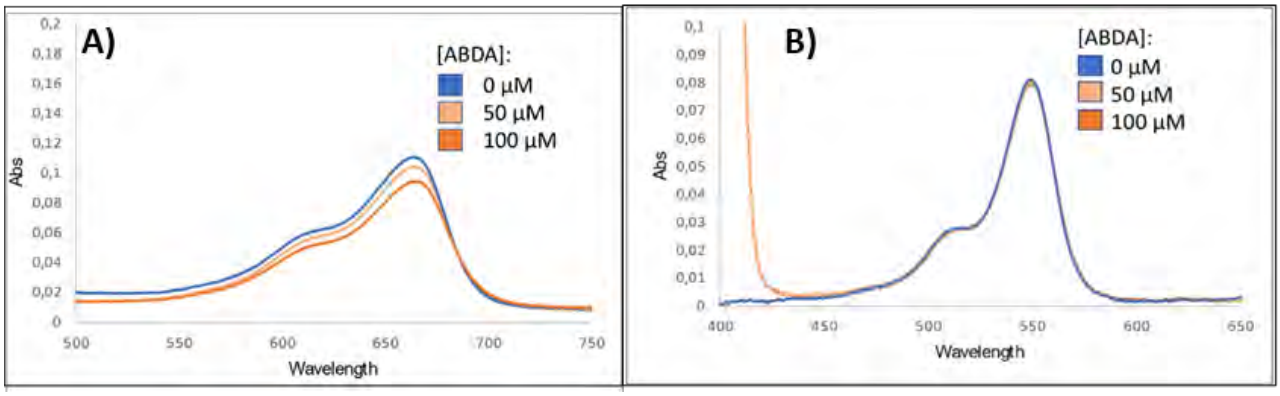

Figure S3. UV spectra of MB (left) and RB (right) at 1 µM concentration, in presence of 0, 50 and 100 µM of ABDA. Experiments performed in Tris Buffer (pH 7.4, 10 mM K^+) at 25°C.

Given the interactions between MB, DNA and ABDA the exact values of singlet oxygen quantum yield (φ) could not be calculated. We therefore refer to "ABDA quenching" rather than φ. The ABDA quenching in presence of DNA was evaluated as follows:

$$\text{ABDA Quenching} = \frac{m_{PS+DNA}}{m_{PS}} \qquad (2)$$

Where m_{PS+DNA}, m_{PS} are the slopes of the logarithmic degradation curves in presence and absence of DNA, respectively.

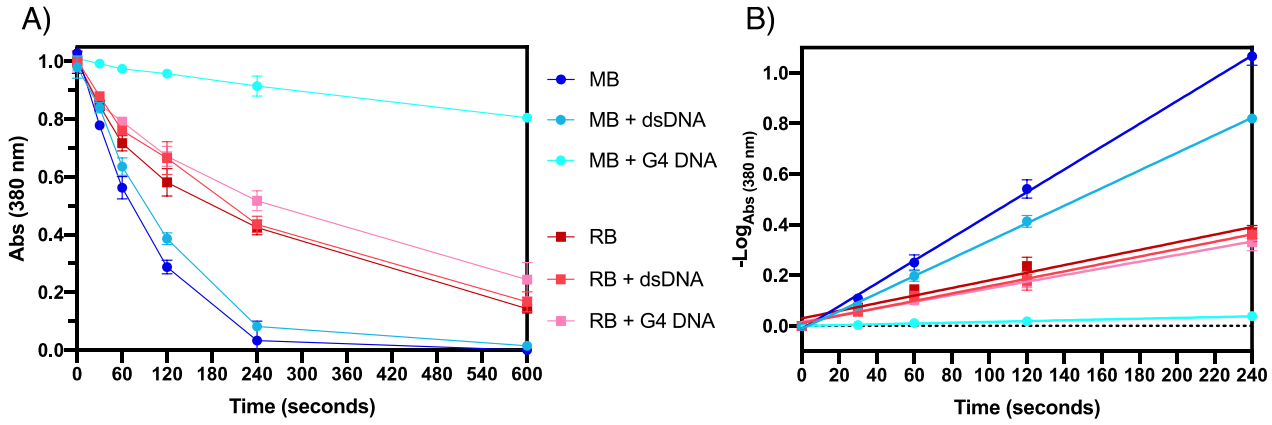

Figure S4. ABDA quenching in presence of **MB** (blue curves) and **RB** (red curves) upon irradiation, in presence or absence of G4 (c-kit WT) and dsDNA (dsDNA A + dsDNA B). A) UV-VIS spectrum recorded at 380 nm; B) Logaritmic plot of the degradation profiles. Experiments are performed at 1.0 µM Photosensitizer, 5.0 µM DNA, and 100 µM ABDA in Tris buffer (pH 7.4, 10 mM K^+) at 25°C.

Table S1. ABDA quenching by irradiation of RB and MB in presence and absence of ds and G4 DNA.

PS	Relative ABDA quenching in presence of dsDNA	Relative ABDA quenching in presence of G4-DNA
MB	0.83 ± 0.02	0.035 ± 0.002
RB	0.97 ± 0.06	0.89 ± 0.1

To evaluate the influence of the interaction between MB and ABDA on ABDA quenching, we performed the ABDA quenching experiment in presence of a less polar solvent system, able to perturb the stacking interaction between the two aromatic systems.[S4] Based on UV spectroscopy experiments, the addition of 10% DMF to the ABDA-containing mixture restored the normal absorption spectrum of MB, thus we can reasonably assume

that π-π interactions are lost (Figure S5A). When performing the quenching experiment under these conditions, we found that the overall effect on ABDA-quenching remains limited (a slightly increased singlet oxygen production is noticed). Despite the reduction of ABDA quenching by MB in presence of G4-DNA, the ligand oxidation rate is increased, thus corroborating the hypothesis of Ligand-MB co-localization (please refer to ESI section 5 "Ligand oxidation experiments").

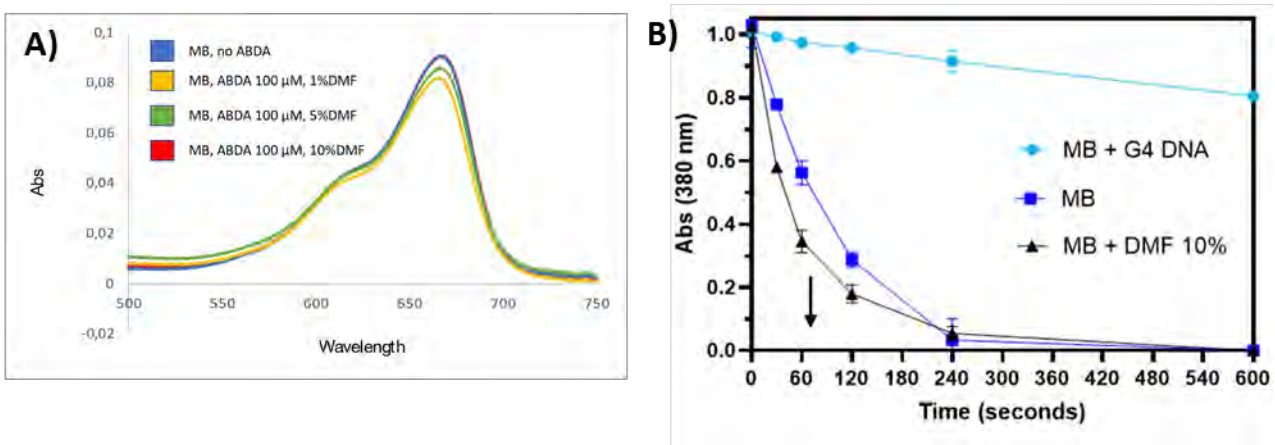

Figure S5. Influence of increasing DMF quantities (blue curve: 0%; yellow curve: 1%; green curve: 5%; red curve:10%) on the UV-Absorption spectra of MB (A) and ABDA quenching experiments as deduced from ABDA absorbance at 380 nm in presence of MB (B). The experiments were performed at 1 µM PS concentration and 100 µM ABDA concentration, in Tris Buffer (pH 7.4, 10 mM K^+) at 25°C.

When G4-DNA is present in the mixture, the level of ABDA quenching by MB irradiation is drastically reduced, although efficient ligand oxidation is maintained even when lowering MB concentration (see section 5). On the other hand, ABDA quenching in presence of RB is not significantly different when G4-DNA is added. The reduced ABDA oxidation is explained by a combination of factors: 1) the stacking of MB onto the guanines of the G-tetrads (supported by the bathochromic shift and the hypochromic effects seen in the UV absorption spectrum); 2) the "sequestration" of MB from the solution (and therefore from oxygen and ABDA) due to the formation of the MB-G4 complex. 3) quenching of the MB excited state by the guanines.[S5] Additionally, modelling studies suggest a binding mode in which the dye is stacked onto the lower tetrad of the quadruplex, thus shielding MB and causing an inefficient energy transfer to molecular oxygen. The reduced singlet oxygen production does not affect the oxidation of the ligand due to its co-localization with MB within the G4-DNA (See section 10.4 for more details). These hypotheses are supported by the fact that in conditions that displace MB from its complex with the G4, ABDA quenching is partially restored (Figure S6). This can be done by performing the ABDA quenching experiments in presence of Mg^{2+} [S6] or by adding a high excess of double-stranded DNA which starts to compete with G4 for MB binding.[S7]

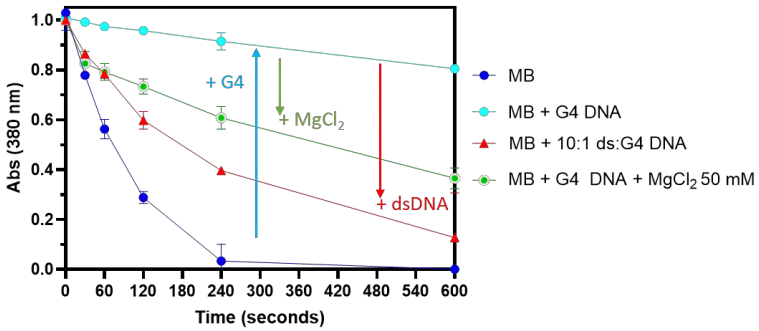

Figure S6. ABDA quenching in presence of MB (dark blue line) and the influence of the presence of G4 DNA (light blue line), a 10:1 mixture of dsDNA and G4-DNA (red line) and G4-DNA + 50mM $MgCl_2$ (green line). Total DNA concentration: 5 µM; ABDA concentration: 100 µM. Experiments performed in Tris HCl buffer (pH 7.4, 10 mM K^+).

4. DNA oxidation studies

Being aware of the previous literature reports indicating oxidative damage and dsDNA cleavage by photo-excitation of MB, [S8] and to evaluate potential damage to G4 and dsDNA at our experimental conditions, we performed a preliminary experiment by irradiating solutions containing different types of DNA in presence of 2.0 μM MB (Figure S7). The absence of detectable oxidative damage is related to the low power of the light used for the irradiation experiment (0.73 W), and the low concentration of photosensitizer. In the earlier literature, the DNA damage was induced by laser irradiation of the samples in presence of a large excess of MB.[S9] Laser irradiation significantly differs from halogen lamp emission due to the high spectral purity (narrow bandwidth, monochromatic emission that can be selected to the absorption window of the PS) and for being a coherent light emission source (which can be focused on a small surface for delivering high surface power density). As a consequence, the effective power delivered to the sample using a halogen set-up is lower as compared to what can be achieved even with a low-end laser.

A 10 μM working solution of PS was prepared from a freshly made 100 μM solution. In a 1.5 mL Eppendorf tube, 300 μL of air saturated buffered solution (Tris HCl 100mM, pH 7.4, 10 mM K^+) containing 5 μM DNA, was prepared and annealed by heating at 95°C for 5 minutes and slowly cooling down to 37°C over a period of 2 hours. The PS was added to the tube at a final concentration of 2.0 μM. The lamp was placed on top of the Eppendorf tube for the entire duration of the experiment (30 minutes). DNA damage was evaluated by HPLC-UV and MALDI-TOF analysis.

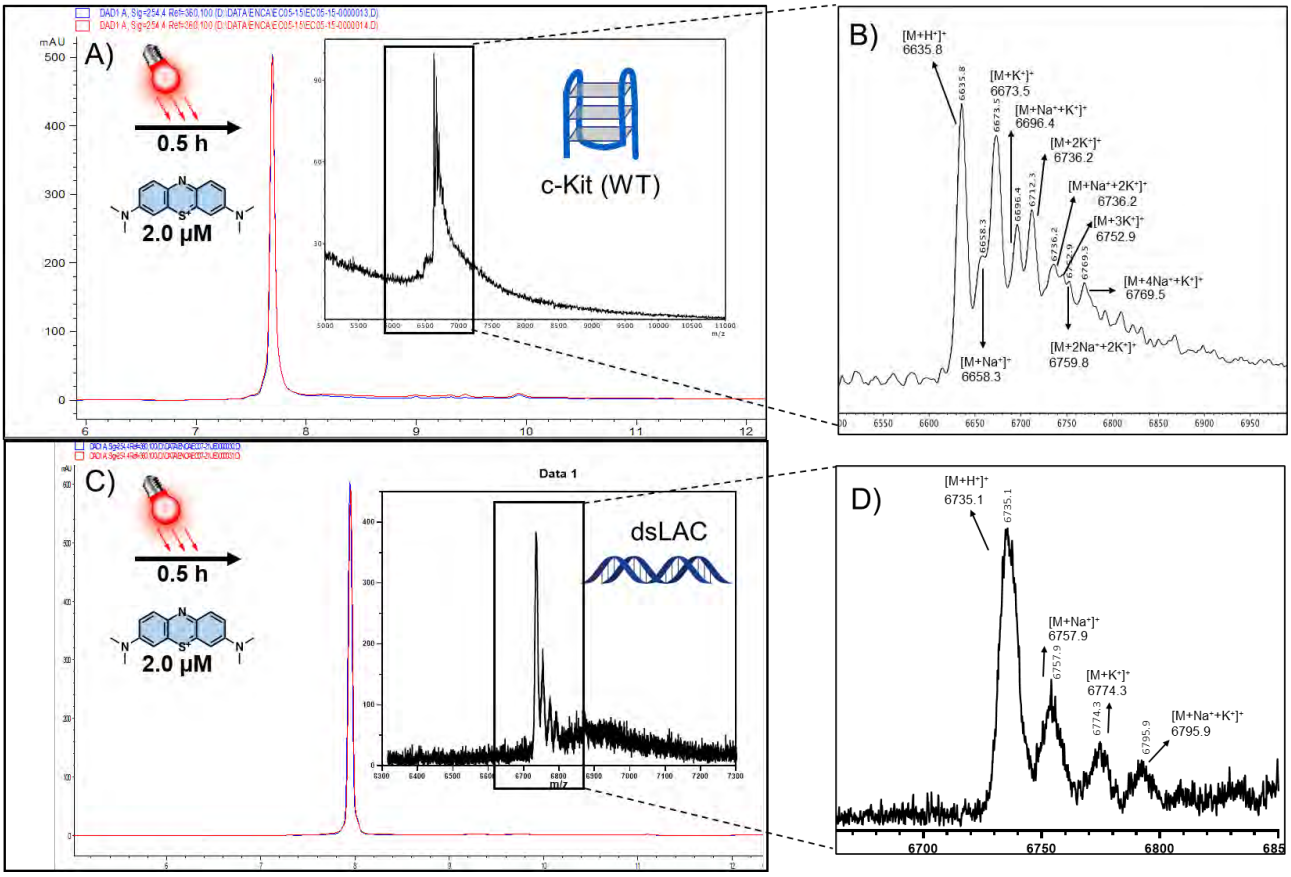

Figure S7. DNA oxidation damage evaluation on c-Kit (A-B) and dsLAC (C-D) in presence of MB at 2.0 μM concentration, at 0 (blue trace) and 30 minutes irradiation (red trace). The inserts (B and D) show MALDI-TOF analysis of the purified DNA peaks. No oxidation of the DNA was observed. The experiment was performed at 5 μM DNA concentration, in buffered solution (Tris HCl, pH 7.4, 10mM K^+).

5. Ligand oxidation experiments

In a typical experiment, a 10 μM working solution of PS was freshly prepared. In a 1.5 mL Eppendorf tube, 300 μL of air saturated buffered solution (Tris HCl 100mM, pH 7.4, 10 mM K^+) containing ligand at 25 μM was

prepared and placed in the Eppendorf thermomixer at 37°C. When needed, DNA (*c-kit*) was added up to 5 µM concentration prior the addition of the ligand and annealed at 95°C for 5 minutes, then cooled down over a period of 2 hours. The PS was added to the tube at desired final concentration. The lamp with the appropriate filter was placed on top of the Eppendorf tube and the sample irradiated for the entire duration of the 20 minutes. 50 µL of solution were sampled at different irradiation times and left to react for two hours at 37°C, shielded from light. Ligand oxidation was followed through integration of the 260 nm absorbance of ligand peaks. Integration was performed using Agilent ChemStation for LC 3D systems software (Rev.B.04.01[481]). Data reported are normalized to integrals at 0 minutes irradiation.

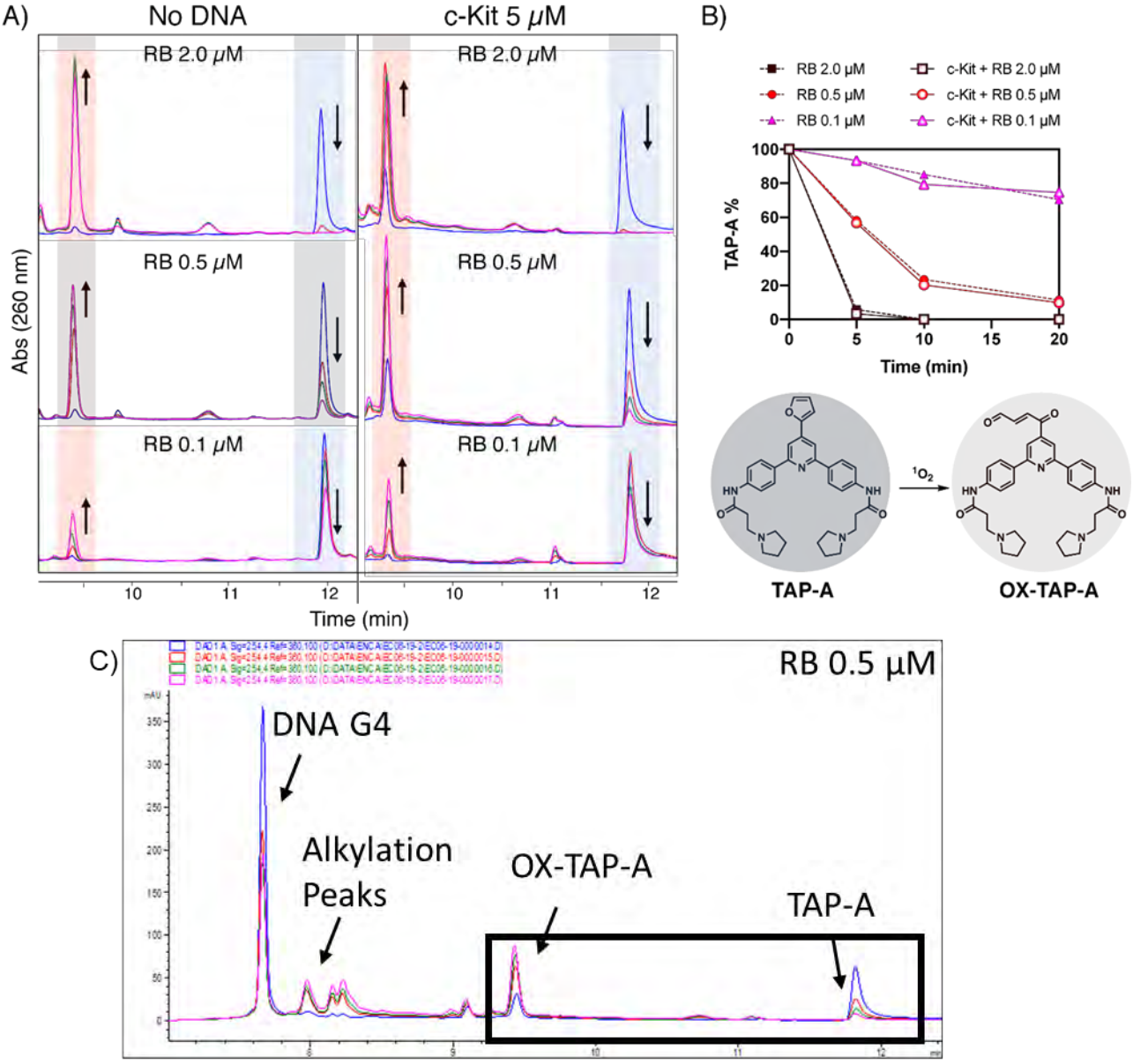

Figure S8. **TAP-A** oxidation profile in presence of **RB** at decreasing concentrations, after 0 (blue), 5 (red), 10 (green) 20 (pink) minutes irradiation, in presence and absence of c-Kit at 5 µM concentration (A). The ligand peak decrease at rt=11.7 min (highlighted in blue) was used to follow the oxidation rate. The peak at rt=9.3 min represents the oxidized species. The data obtained are normalized to integrals at 0 minutes irradiation and plotted on the graph (B). All the chromatograms shown in the figure are sections of the full chromatograms, showing the region between rt=9.2 min and rt=12.2 min, as depicted in panel (C). The experiment was performed at 25µM **TAP-A** concentration, in Tris buffer (pH 7.4, 10 mM K^+), at 25°C.

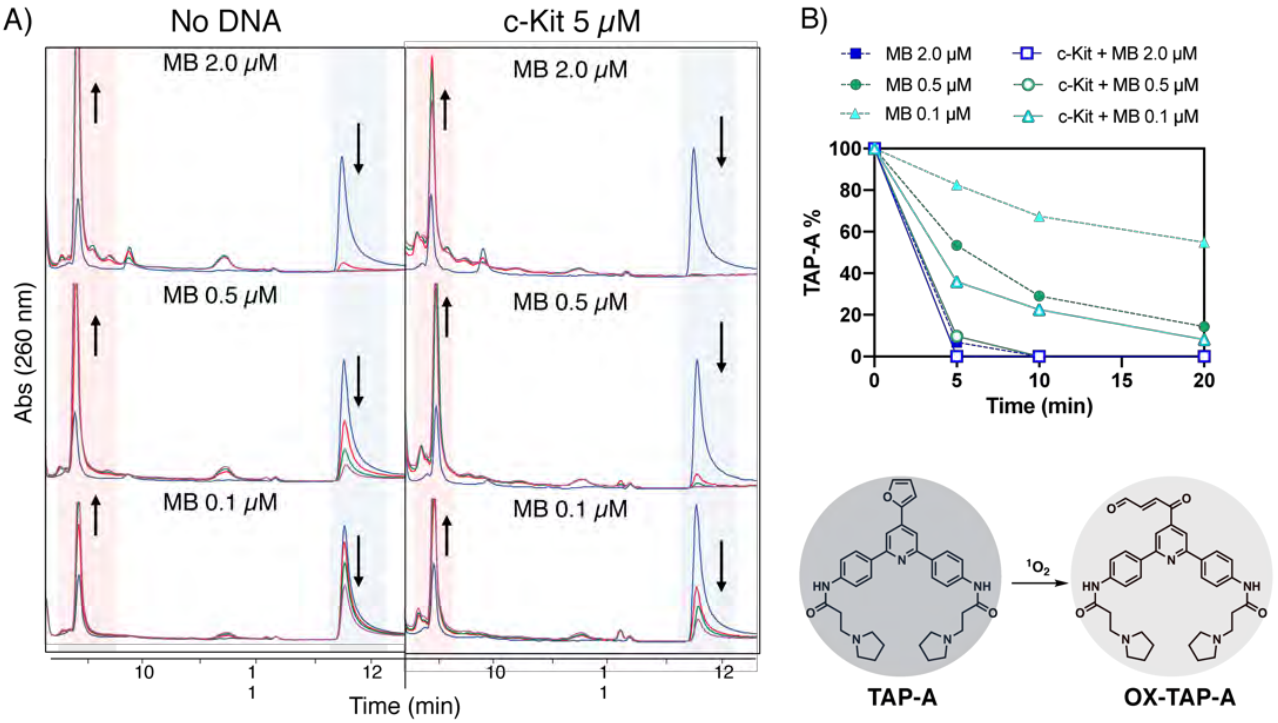

Figure S9. **TAP-A** oxidation profile in presence of **MB** at decreasing concentrations, after 0 (blue), 5 (red), 10 (green) 20 (pink) minutes irradiation, in presence and absence of c-Kit at 5 μM concentration (A). The ligand peak decrease at rt=11.7 min (highlighted in blue) was used to follow the oxidation rate. The peak at rt=9.3 min represents the oxidized species. The data obtained are normalized to integrals at 0 minutes irradiation and plotted on the graph (B). The experiment was performed at 25μM **TAP-A** concentration, in Tris buffer (pH 7.4, 10 mM K^+), at 25°C.

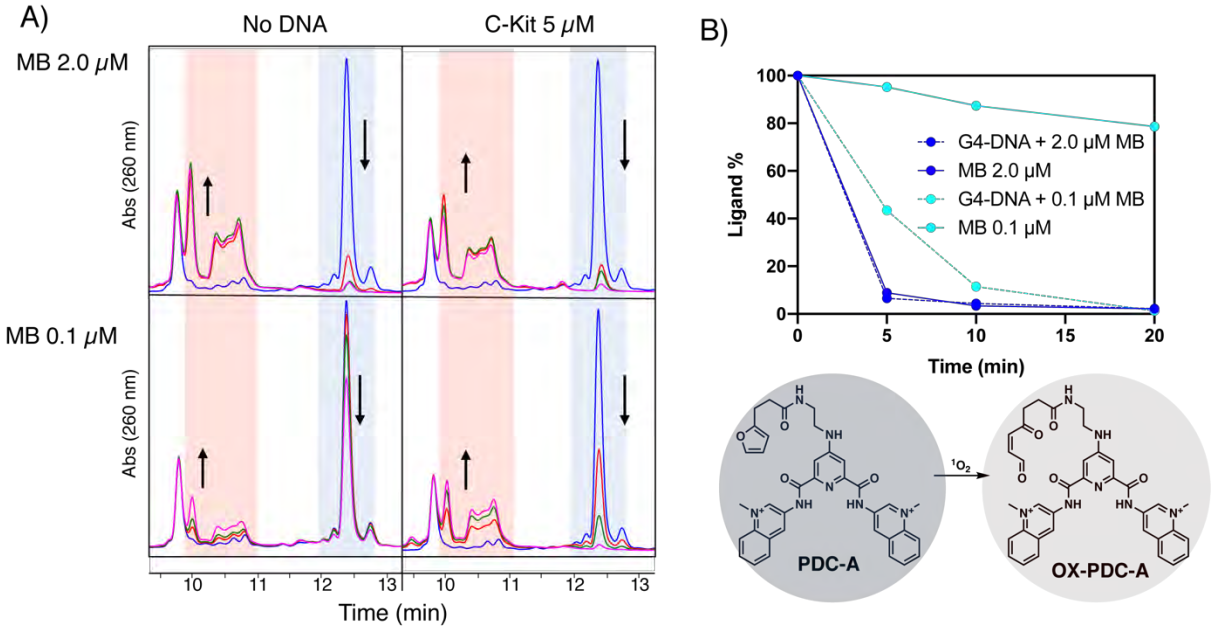

Figure S10. **PDC-A** oxidation kinetics at different concentrations, in presence (A) or absence (B) of 5 μM DNA (c-Kit WT) concentration after 0 (blue), 5 (red), 10 (green) 20 (pink) minutes irradiation. The ligand peak decrease at rt=12.4 min (highlighted in blue) was used to calculate the kinetics. The peaks appearing in the region rt= 10-11 min represent the oxidized species. The data obtained are normalized to integrals at 0 minutes irradiation and plotted on the graph (C). The experiment was performed at 25μM **PDC-A** concentration, in Tris buffer (pH 7.4, 10 mM K^+), at 25°C.

6. Alkylation experiments

In a typical experiment, a 10 μM working solution of PS was freshly prepared. In a 1.5 mL Eppendorf tube, 300 μL of an air saturated buffered solution (Tris HCl 100mM, pH 7.4, 10 mM K^+) containing DNA at 5 μM concentration was prepared and placed in the Eppendorf thermomixer at 95°C for 5 minutes. The solution was slowly cooled down to 37°C over a period of 2 hours, and the ligand was added at a final concentration of 25 μM, and the solution incubated for 30 minutes. **MB** was added to the tube at a final concentration of 0.1 μM or 2.0 μM. The lamp, equipped with a red filter, was placed on top of the Eppendorf tube for the entire duration of the experiment (30 minutes). 50 μL samples of solution were collected at different irradiation times and left to react for two hours at 37°C, shielded from light. The peaks formed upon irradiation are isolated by HPLC, freeze-dried and analyzed via MALDI-TOF.

Table S2. DNA sequences used for alkylation studies.

DNA name	**Sequence (5' – 3')**	**Type**
c-KIT WT	CGGGCGGGCGCGAGGGAGGGT	Anti-parallel G4
c-KIT mut	CGGGCG**AA**CGCGAGGGAGGGT	Mutated G4 (ssDNA)
h-TELO WT	AGGGTTAGGGTTAGGGTTAGGG	Mixed topology G4
h-TELO mut	AGGGTTAG**A**GTTAGAGTTAGGG	Mutated G4 (ssDNA)
c-MYC WT	TGGGGAGGGTGGGGAGGGTGGGGAAGG	Parallel-G4
c-MYC mut	TGGGGAGGGTGG**AA**AGGGTGGGGAAGG	Mutated G4 (ssDNA)
dsDNA 26mer A	CAATCGGATCGAATTCGATCCGATTG	dsDNA
dsDNA 26mer B	GTTAGCCTAGCTTAAGCTAGGCTAAG	
ds Lac	GAATTGTGAGCGCTCACAATTC	dsDNA
ds T-loop	TATAGCTATATTTTTTTATAGCTATA	dsDNA (stem-loop)

6.1. Alkylation studies with C-Kit

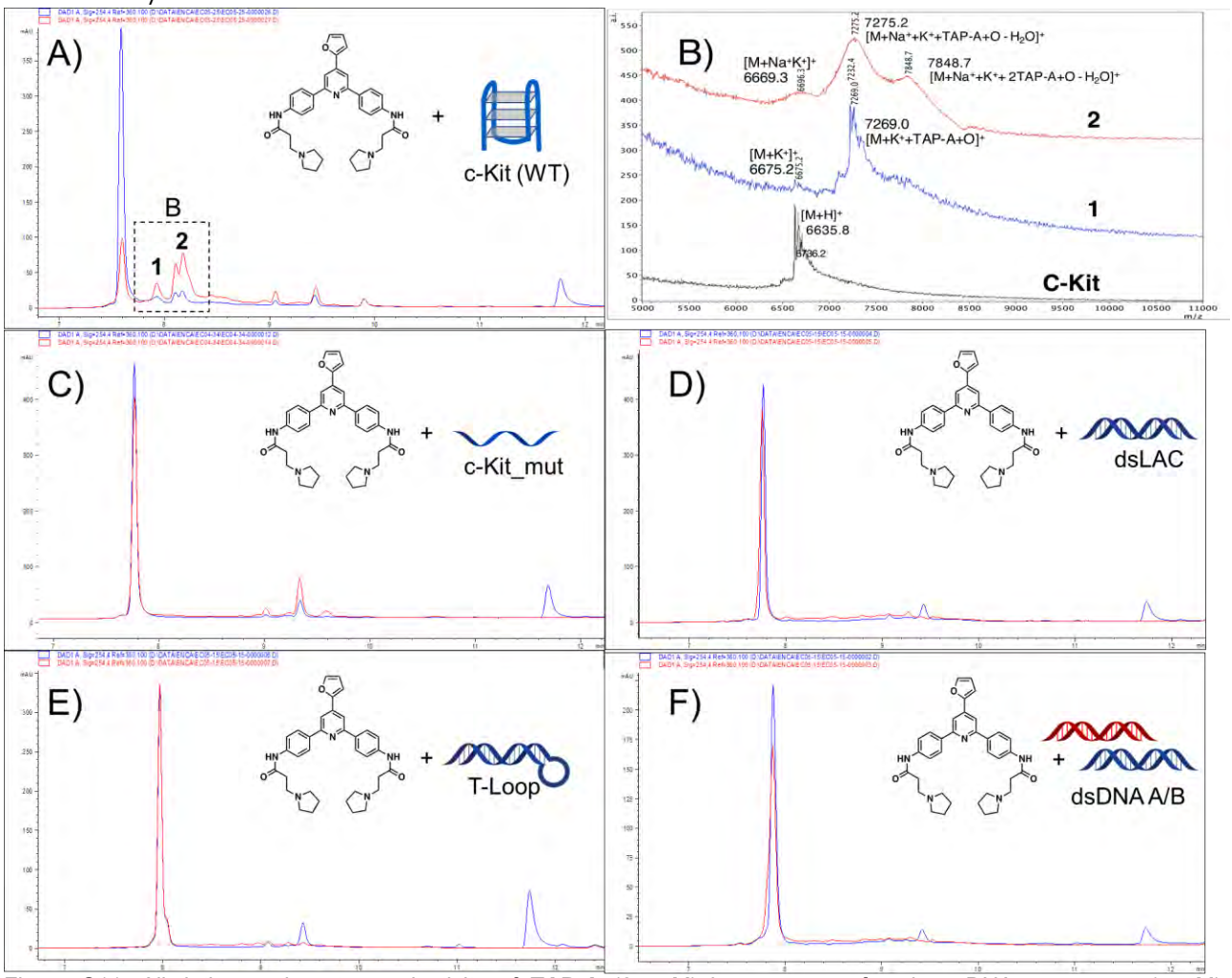

Figure S11. Alkylation and system selectivity of **TAP-A** (25 μM) in presence of various DNA sequences (5 μM). Chromatograms show the reaction mixture at 0 (blue curve) and 30 minutes irradiation (red curve). A) G4 DNA (C-Kit WT),

and MALDI-TOF analysis of the peaks 1 (rt=7.8 min) and 2 (rt=8.2 min) (B); C) dsDNA A + dsDNA B; D) dsLAC; E) t-loop; (F) ssDNA (c-Kit Mut). MB concentration used is 0.1 μM in (A) and 2 μM in (C-F). The experiment was performed in Tris buffer (pH 7.4, 10 mM K^+), at 25°C.

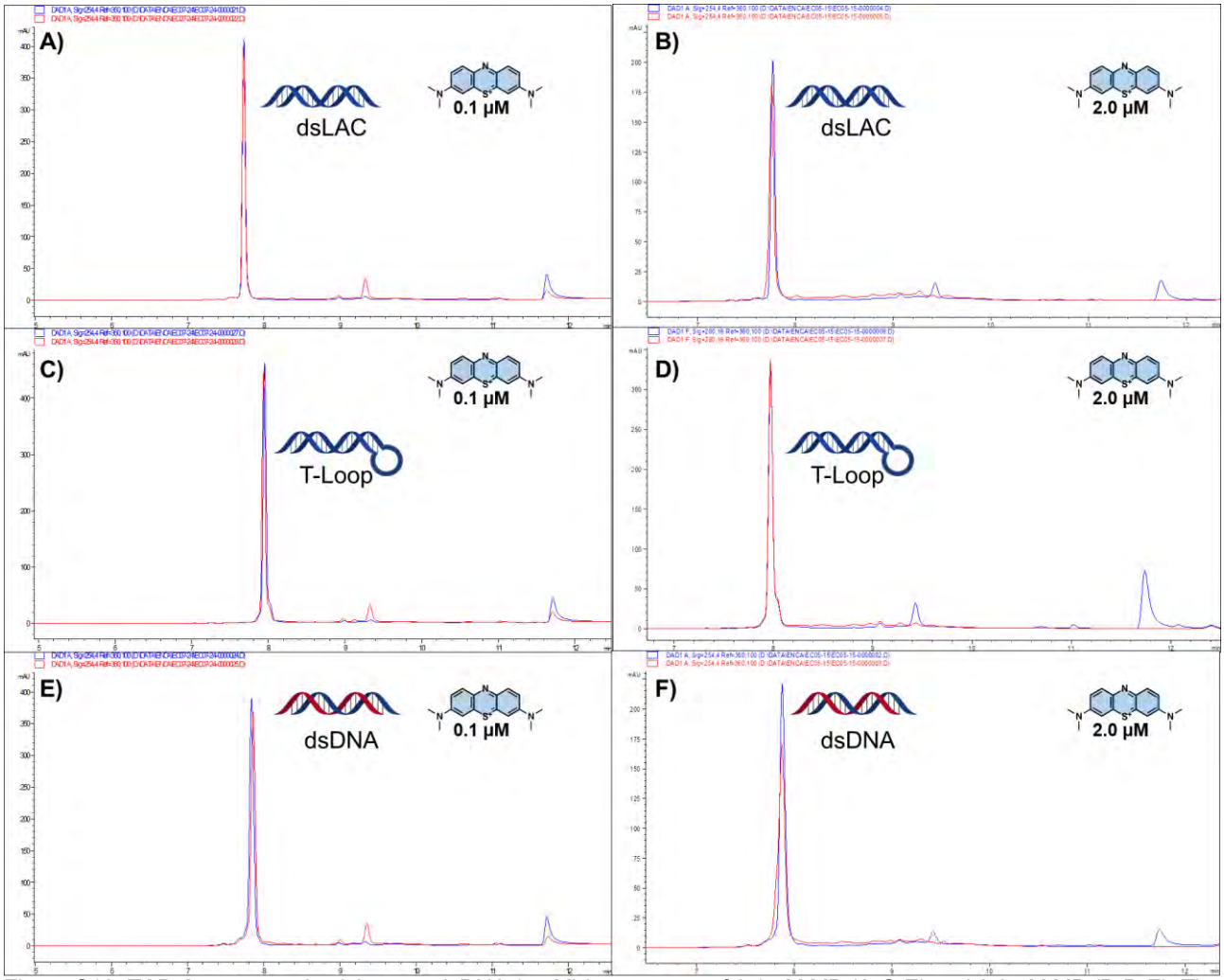

Figure S12. **TAP-A** system selectivity over dsDNA (5 μM) in presence of 0.1 μM MB (A-C-E) and 2.0 μM MB (B-D-F). The activation of the ligand when using 0.1 μM MB A-B) dsLAC; C-D) T-Loop; E-F) dsDNA 26mer. The experiment was performed at 25μM **TAP-A** concentration, in Tris buffer (pH 7.4, 10 mM K^+), at 25°C.

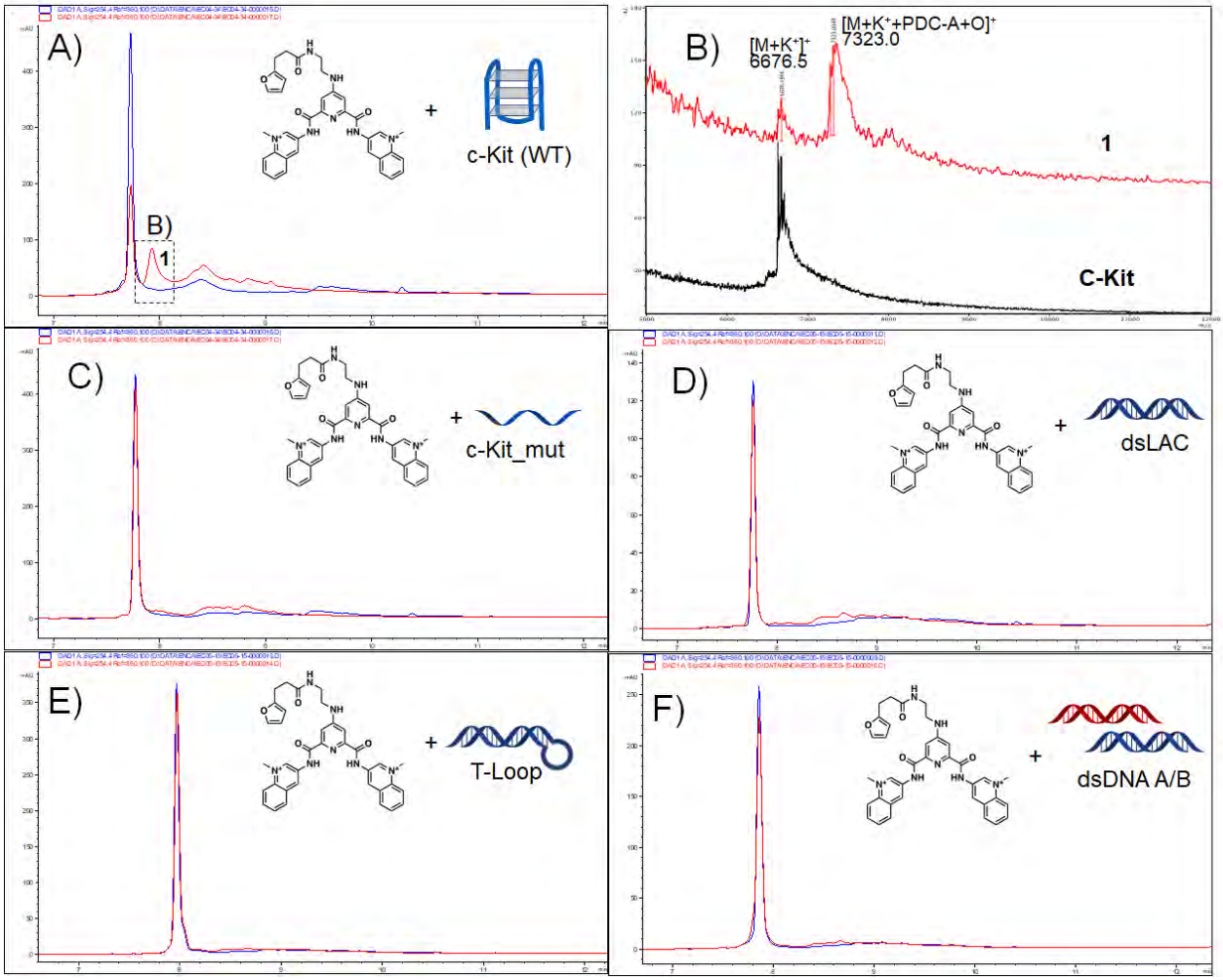

Figure S13. Alkylation and system selectivity of **PDC-A** (25 μM) in presence of various DNA sequences (25 μM)**.** Chromatograms show the reaction mixture at 0 (blue curve) and 30 minutes irradiation (red curve).The first peak appearing in the region rt=7-8 min corresponds to the starting DNA peak. A) G4 DNA (C-Kit WT), and MALDI-TOF analysis of the peak at rt= 7.8 min (B); C) dsDNA A + dsDNA B; D) dsLAC; E) t-loop; (F) ssDNA (c-Kit Mut).

6.2. UV-Absorption spectra

UV-vis spectra of the species involved in the alkylation reaction were extracted from the HPLC-UV chromatogram using Agilent ChemStation for LC 3D systems software (Rev.B.04.01[481]). Each peak corresponding to DNA, ligands, oxidized ligands and alkylation products was selected, and the full UV-vis spectra (200-760 nm) extracted. Data regarding **PDC-A** and **Ox-PDC-A** are extrapolated from ligand oxidation kinetic studies performed in section 5.

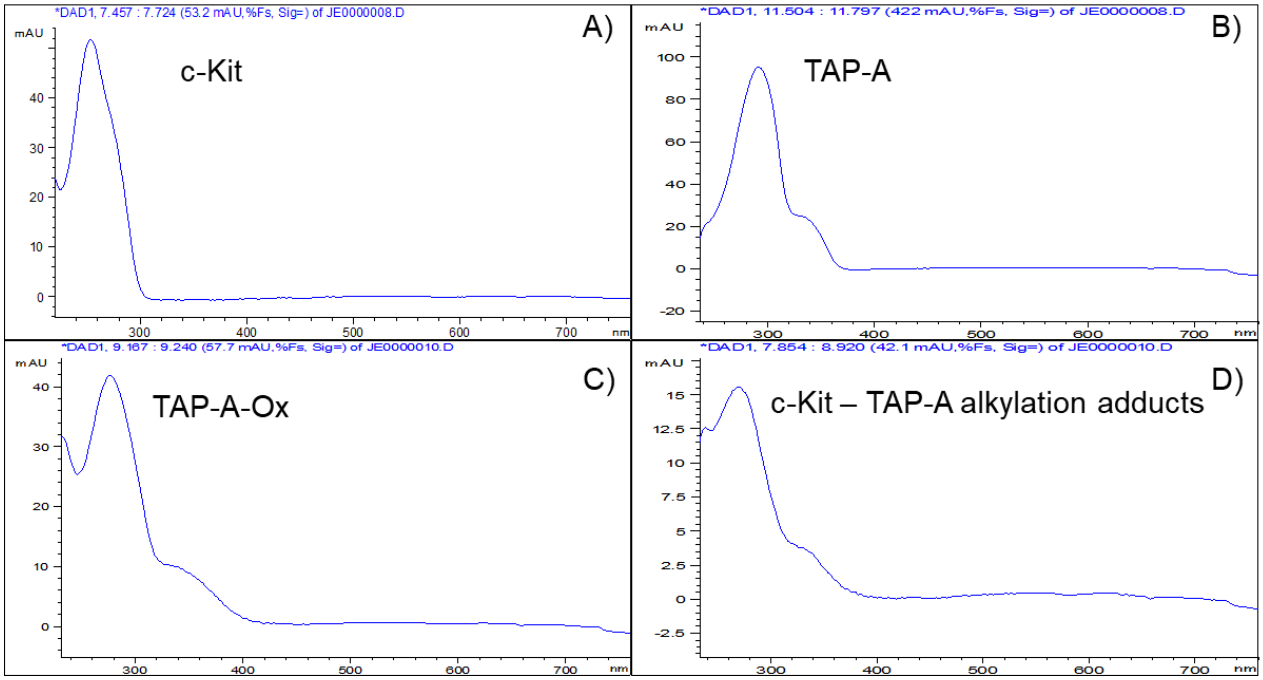

Figure S14. UV spectra of the components of a typical alkylation experiments of c-Kit in presence of TAP-A. A) c-Kit DNA, rt= 7.6 min; B) TAP-A at 0' irradiation time, rt=11.7 min; C) Oxidized TAP-A at 30' irradiation time, rt=9.3 min; D) alkylation adducts of c-Kit and TAP-A (rt= 7.8 to 8.5 min).

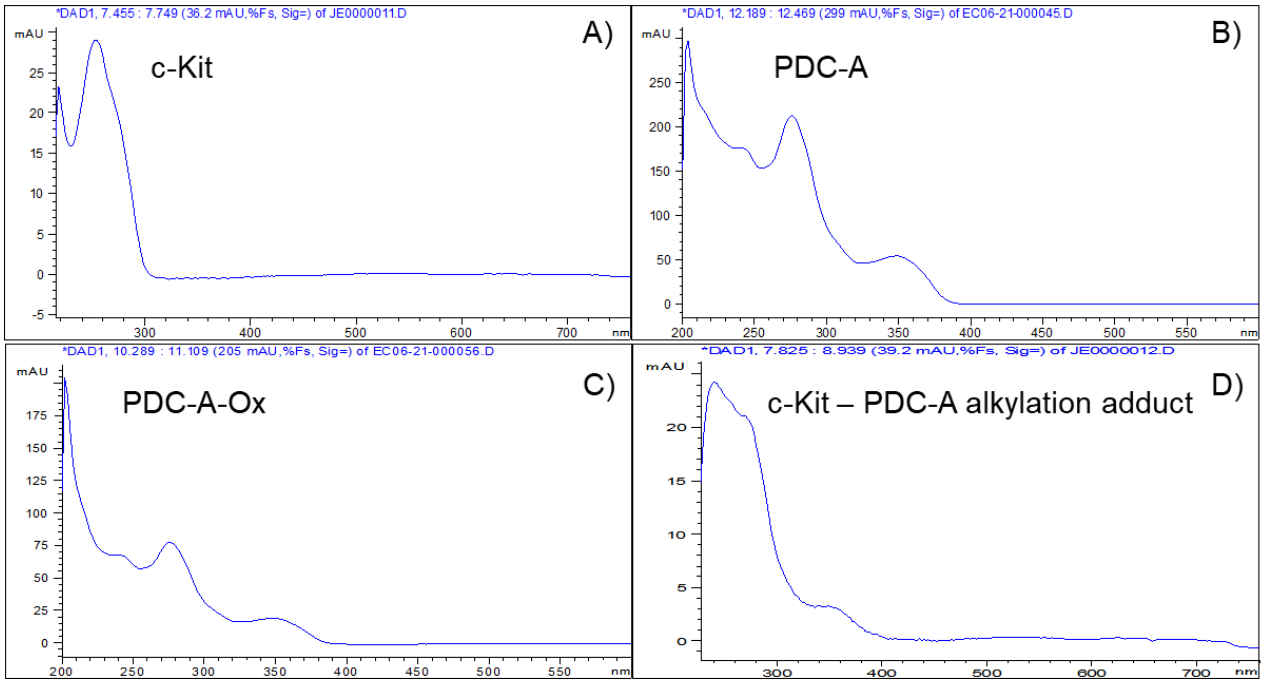

Figure S15. UV spectra of the components of a typical alkylation experiments of c-Kit in presence of PDC-A. A) c-Kit DNA, rt= 7.6 min; B) PDC-A at 0' irradiation time, rt=12.4 min (*); C) Oxidized TAP-A at 30' irradiation time, rt=10-11 min (*); D) alkylation adducts of c-Kit and PDC-A (rt= 7.8 to 8.5 min).* *Data extrapolated from the PDC-A oxidation experiment depicted in Figure S10 (please refer to section 5).*

7. Loop residue substitution

7.1. Preliminary UV-melting experiments

The formation of a stable G4 structure was evaluated by UV-melting, monitoring the absorbance at 295 nm. To ensure the formation of only the most stable structure, the samples were pre-annealed at 95°C for 5 minutes and cooled to 15°C with a heating rate of 1°C/min. The experiments were carried out from 15°C to 95°C and from 90 °C to 15 °C with a heating/cooling rate of 1 °C/min and recording every 0.1 °C. DNA concentration was kept at 5 μM, in pH 7.4 PBS Buffer (10 mM KCl, 100 mM phosphate). Melting temperatures were calculated from the first order derivative of a 10th order polynomial fitting function.

Table S3. Sequences used for the loop residue substitution experiment. The substitution is highlighted in bold.

Name	**Sequence (5' → 3')**	**Substitution**	**T_M (°C)**
c-kit WT	CGGGCGGGCGCGAGGGAGGGT	Wild-type sequence	49.7 ± 1.1
c-kit T1	**T**GGGCGGGCGCGAGGGAGGGT	C1-T	48.0 ± 1.2
c-kit T5	CGGG**T**GGGCGCGAGGGAGGGT	C5-T	53.0 ± 1.3
c-kit T9	CGGGCGGG**T**GCGAGGGAGGGT	C9-T	49.1 ± 1.3
c-kit T10	CGGGCGGGC**T**CGAGGGAGGGT	G11-T	46.43 ± 2.1
c-kit T11	CGGGCGGGCG**T**GAGGGAGGGT	C11-T	52.9 ± 1.6
c-kit T12	CGGGCGGGCGC**T**AGGGAGGGT	G12-T	47.5 ± 1.2
c-kit T13	CGGGCGGGCGCG**T**GGGAGGGT	A13-T	48.3 ± 1.3
c-kit T17	CGGGCGGGCGCGAGGG**T**GGGT	A17-T	55.0 ± 1.6
c-kit LT	**T**GGG**T**GGG**TTTTT**GGG**T**GGGT	All residues in loops substituted by thymine	50.8 ± 1.1

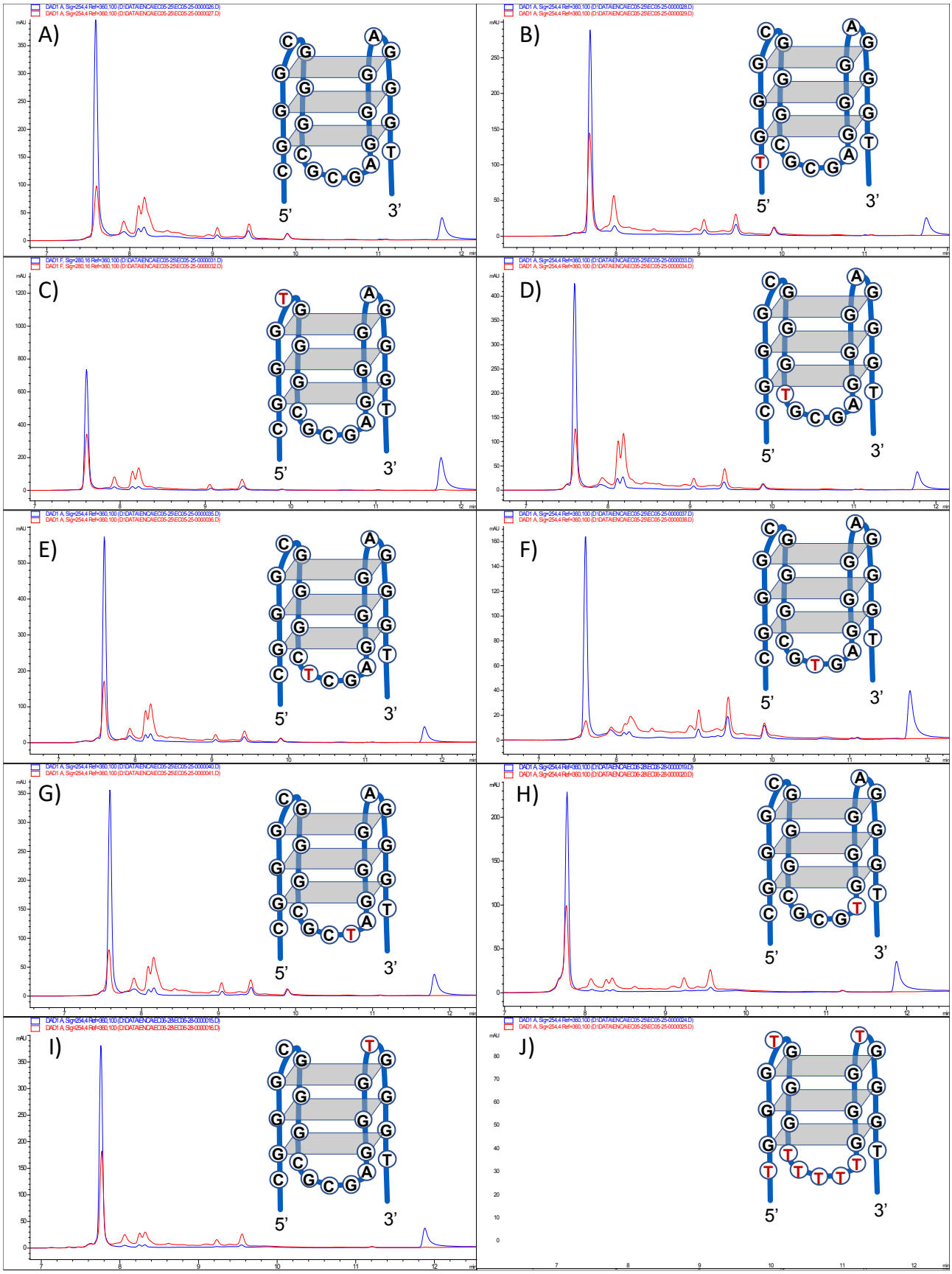

Figure S16. Effect of loop residue substitution (5 μM DNA concentration), in presence of **TAP-A** (25 μM) and **MB** as photosensitizer (0.1 μM), before (blue curve) and after 30' irradiation (red curve). A) c-kit WT; B) c-kit 1T; C) c-kit 5T; D) c-kit 9T ; E) c-kit 10T; F) c-kit 11T; G) c-kit 12T; H) c-kit 12T; I) c-kit 13T; J) c-kit LT. The experiment was performed in Tris buffer (pH 7.4, 10 mM K^+), at 25°C.

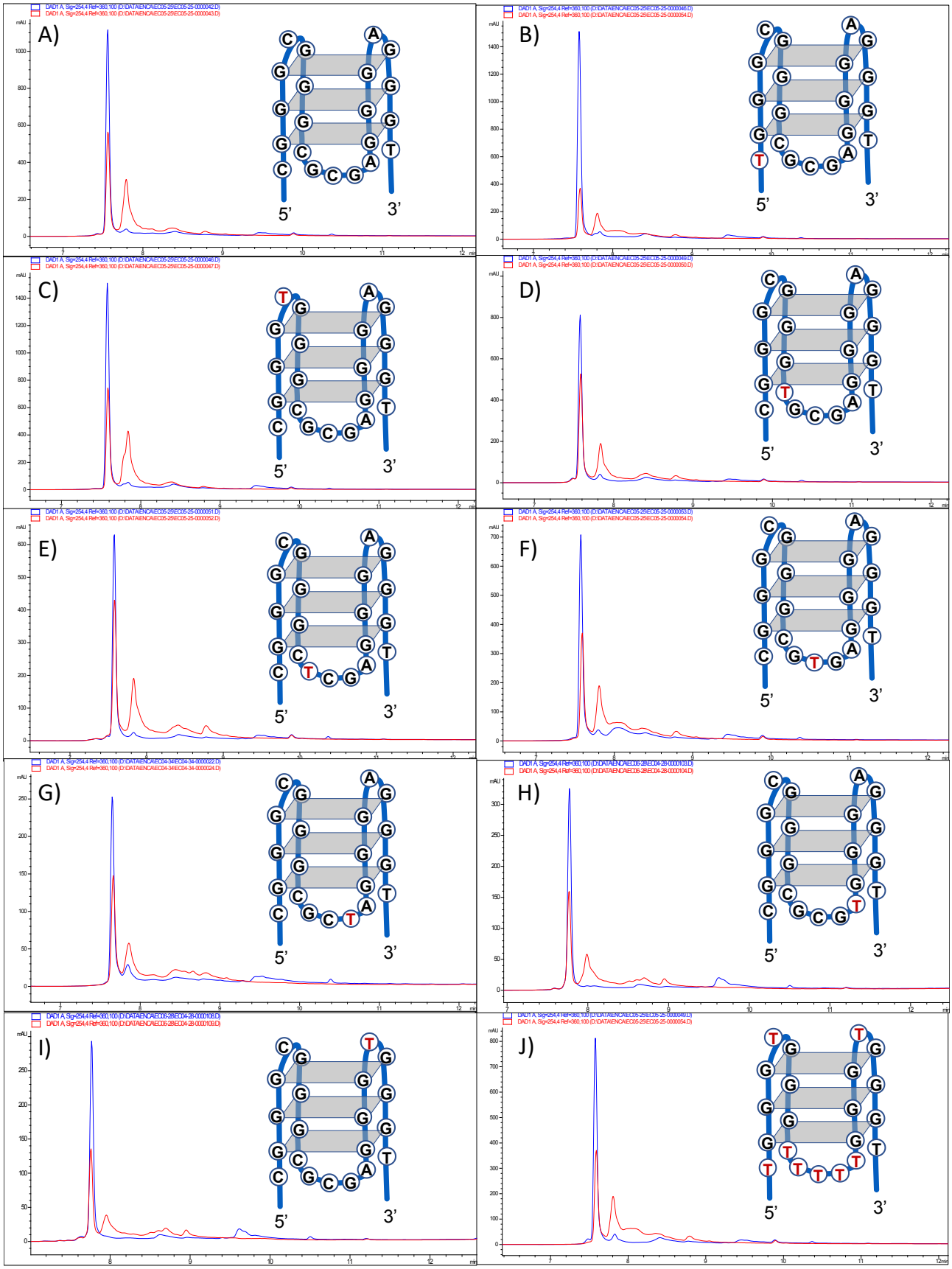

Figure S17. Alkylation experiments showing the effect of loop residue substitution (5 μM DNA concentration), in presence of **PDC-A** (25 μM) and **MB** as photosensitizer (0.1 μM), upon no irradiation (blue curve) and 30' irradiation (red curve). A) c-kit WT; B) c-kit 1T; C) c-kit 5T; D) c-kit 9T ; E) c-kit 10T; F) c-kit 11T; G) c-kit 12T; H) c-kit 12T; I) c-kit 13T J) c-kit LT. The experiment was performed in Tris buffer (pH 7.4, 10 mM K^+), at 25°C.

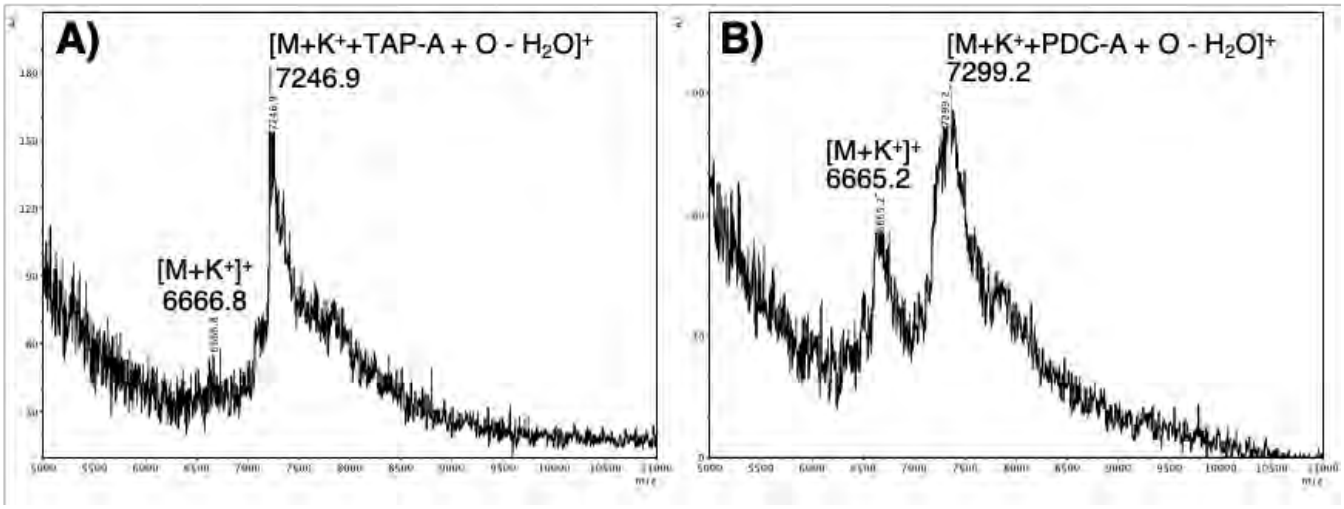

Figure S18. MALDI-TOF analysis of the purified alkylation peaks after reaction with c-Kit LT (refer Figure 4 in the manuscript). A) MALDI-TOF spectrum of TAP-A + c-Kit LT; B) MALDI-TOF spectrum of PDC-A + c-Kit LT.

8. Ligand oxidation studies and alkylation in presence of competing dsDNA

In a typical experiment, a 10 μM working solution of PS was freshly prepared. In a 1.5 mL Eppendorf tube, 300 μL of air saturated buffered solutions containing DNA c-Kit at 5 μM and dsDNA (dsLAC) at 0 μM, 5 μM, 25 μM and 50 μM were prepared and placed in the Eppendorf thermomixer at 95°C for 5 minutes. The solutions were then slowly cooled down to 37°C over a period of 2 hours, and **TAP-A** was added at a final concentration of 25 μM, and the solutions incubated for 30 minutes at 37°C before the addition of MB at a final concentration of 0.2 μM. The lamp, equipped with a red filter, was placed on top of the Eppendorf tube for the entire duration of the experiment (30 minutes). Ligand oxidation and c-Kit consumption were followed through integration of the 260 nm absorbance of ligand peaks. Integration was performed using Agilent ChemStation for LC 3D systems software (Rev.B.04.01[481]). Data reported are normalized to integrals at 0 minutes irradiation.

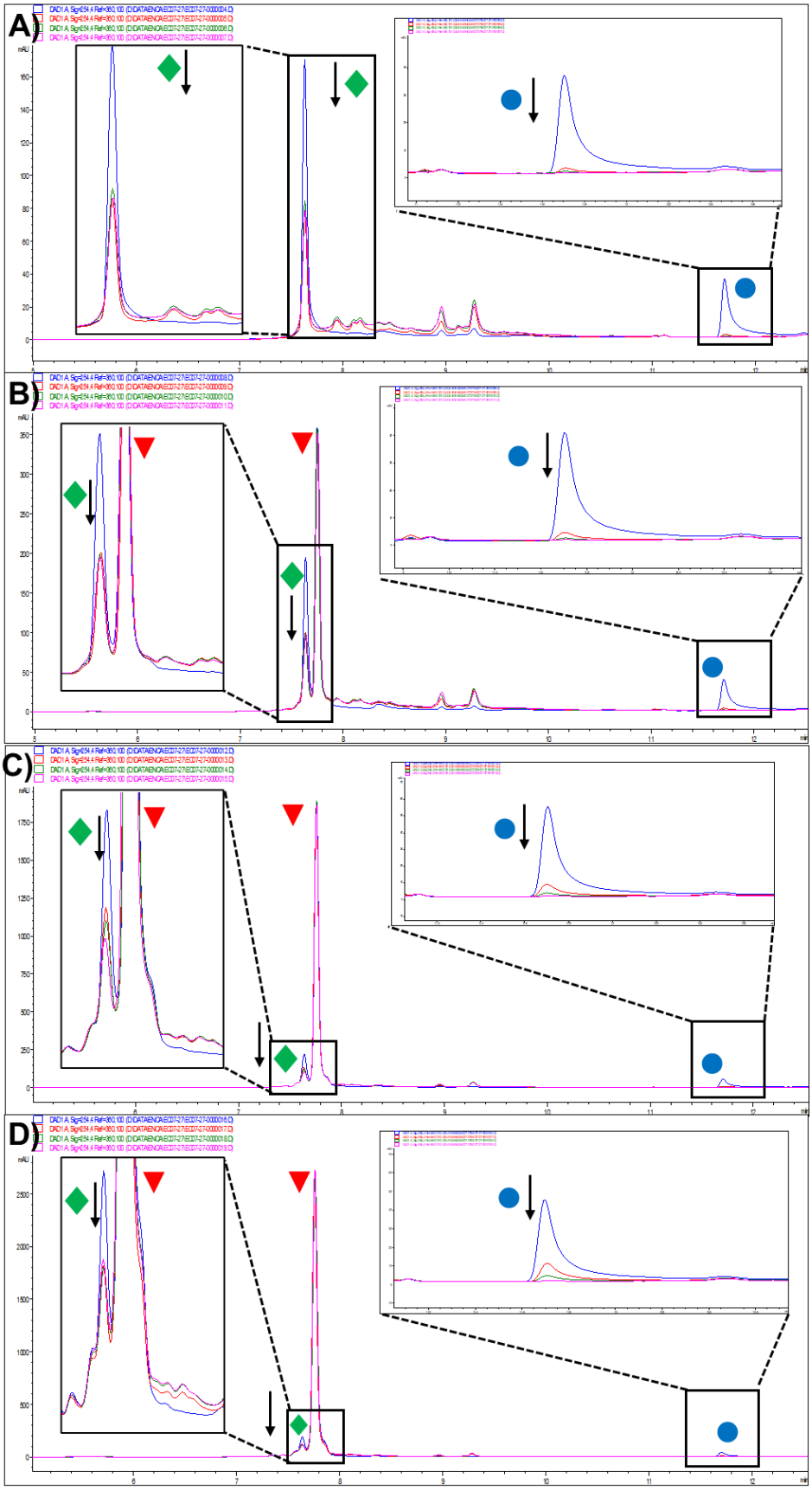

Figure S19 Competition experiment showing the effect on **TAP-A** activation (blue circle ●) and c-Kit consumption (green diamond ♦) in presence of increasing concentrations of competing dsDNA (dsLAC, red triangle ▼), at various irradiation time points (blue: 0'; red: 10'; green: 20'; pink: 30'). C-Kit concentration is maintained constant at 5.0 µM A) no dsLAC ; B) dsLAC 5 µM; C) dsLAC 25 µM; D) dsLAC 50 µM. The experiment was performed in Tris buffer (pH 7.4, 10 mM K^+), at 25°C.

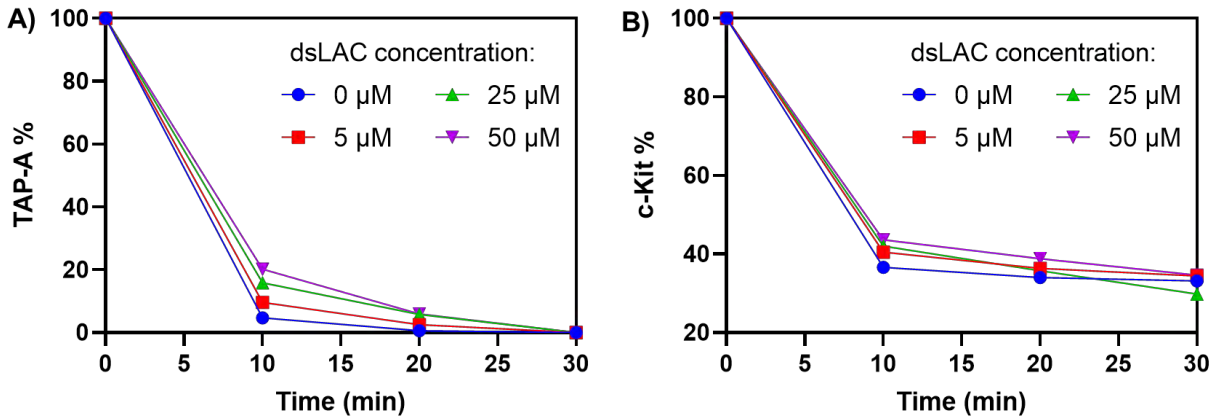

Figure S20. Graph showing the **TAP-A** oxidation rate (A) and c-Kit conversion rate (B) extrapolated from figure S19. The data obtained are normalized to integrals at 0 minutes irradiation and plotted on the graph.

9. Alkylation studies with other sequences and ligands

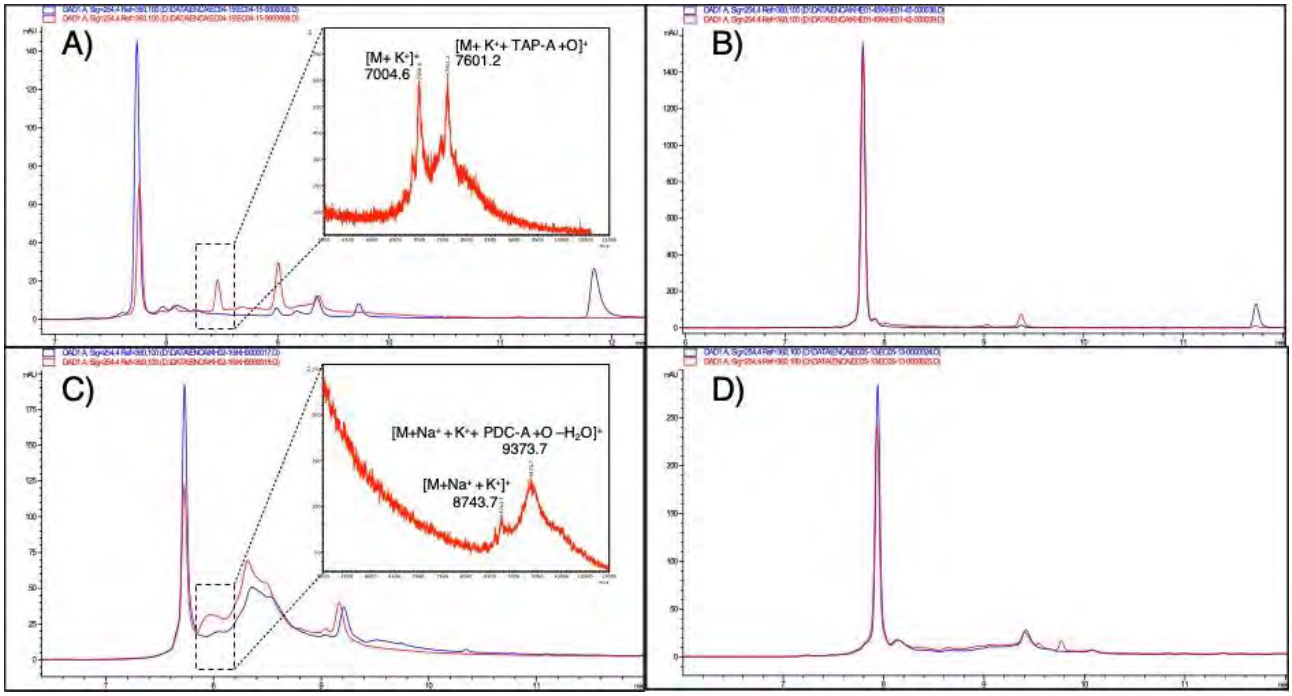

Figure S21. Alkylation and system selectivity of **TAP-A** (A-B) and **PDC-A** (C-D) at 25 μM concentration, in presence of 5 μM DNA. Chromatograms show the reaction mixture at 0 (blue curve) and 30 minutes irradiation (red curve). A) h-telo (WT) and MALDI-TOF spectra of the isolated peak; B) h-telo_mut; C) c-Myc (WT); D) c-Myc_mut.

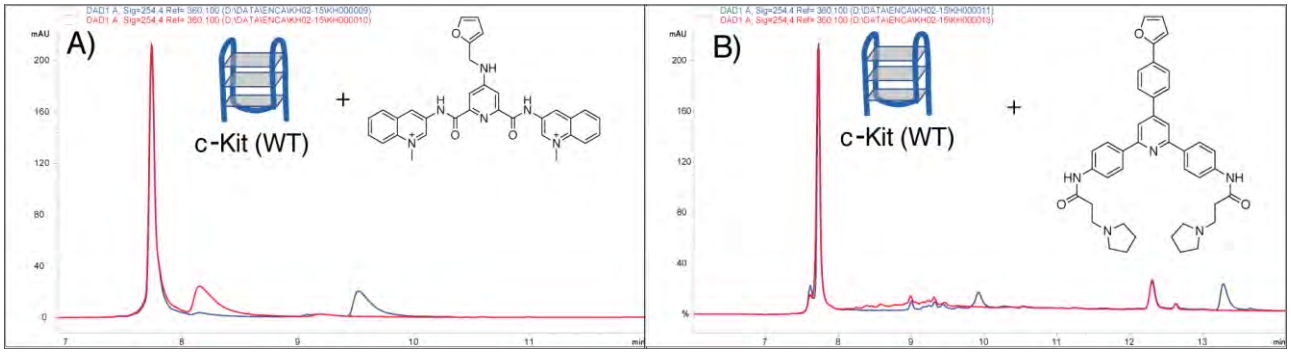

Figure S22. Alkylation experiment performed with **TAP-B** (A) and **PDC-B** (B), at 25 μM concentration, in presence of c-Kit (WT) G4-forming sequence. No alkylation adducts were found.

10. Modeling Data

10.1. Method

TAP-A, PDC-A, TAP-B and PDC-B ligands and MB were built within the Avogadro molecular editor.[S10] Molecular mechanics calculations were then performed to optimize the geometry of the ligands. For this, a two-step minimization procedure, i.e., a steepest descent optimization followed by a conjugate gradient optimization, was performed with the General Amber Force Field (GAFF).[S11] The energy convergence criterion was set at 10^{-5} kJ·mol^{-1} for the energy minimization. The coordinates of the c-kit G-quadruplex were obtained from the Protein Data Bank (PDB ID: 2KQH). Different NMR conformations were extracted to perform ensemble docking calculations, i.e., 10 conformations in the case of the 2KQH target. Docking calculations were performed with *QuickVina-W*, a fork of the well-known Autodock Vina package, adapted for wide search space and blind docking.[S12] As we have no *a priori* knowledge of ligand binding modes in the c-kit structure, a sufficiently large grid was built around each G4 conformer to allow the exploration of the entire G4 surface during the docking calculations. A grid size of 50 × 50 × 50 Å^3 with a spacing of 1.0 Å was thus considered. The center of the grid box was located on the center-of-mass of the c-kit target. As the grid presents an important size in our blind docking protocol, an exhaustiveness value of 64 was chosen, a larger one than the default value (i.e. 8).[S13] Ligands were set as flexible molecules. Particularly, we considered torsions between aromatic moieties and along alkyl chains. The 10 most energetically favorable complexes were retained for each docking calculation. The PyMOL molecular visualization system was utilized to illustrate the ligands binding modes. [S12]

10.2. Supporting data

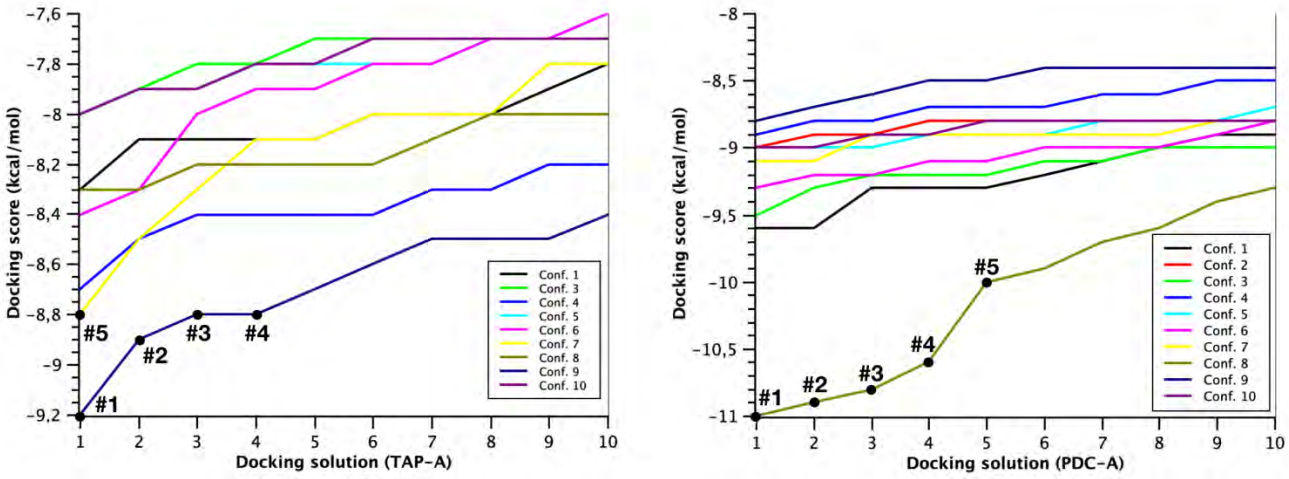

Figure S23. Energy scores of the ten recorded docking solutions for **TAP-A** (left) and **PDC-A** (right) ligands according to each conformer issued from the NMR coordinates of c-kit (PDB ID: 2KQH).

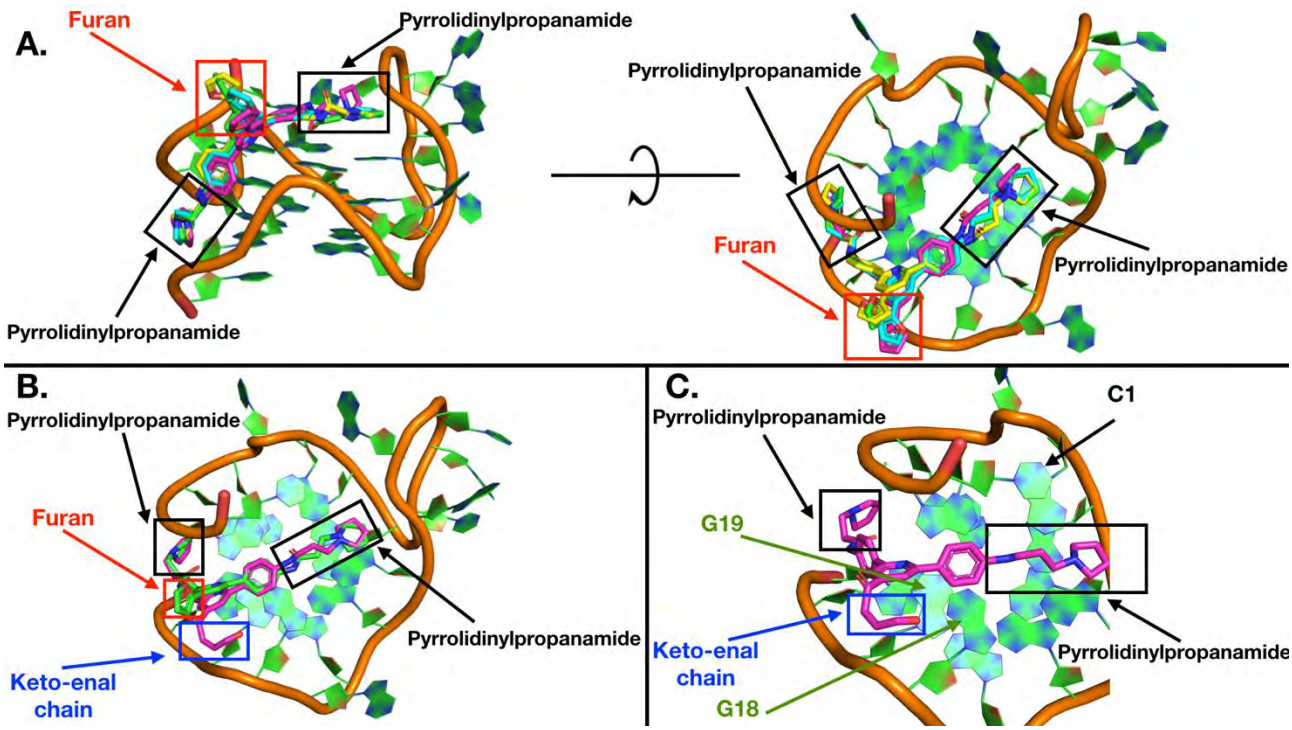

Figure S24. (A) Superimposition of the four best **TAP-A** docking solutions (furan-closed forms of **TAP-A**) as obtained with the c-kit conformer #9. (B) Superimposition of the best ranked **TAP-A** docking solutions for the furan-closed (green ligand) and oxidized (magenta ligand) forms of the ligand, as obtained with the c-kit conformer #9. (C) Best **TAP-A** docking solution for the oxidized form of the ligand. One pyrrolidinylpropanamide chain is located on top of the upper quartet next to C1, whereas the second chain is docked in the groove.

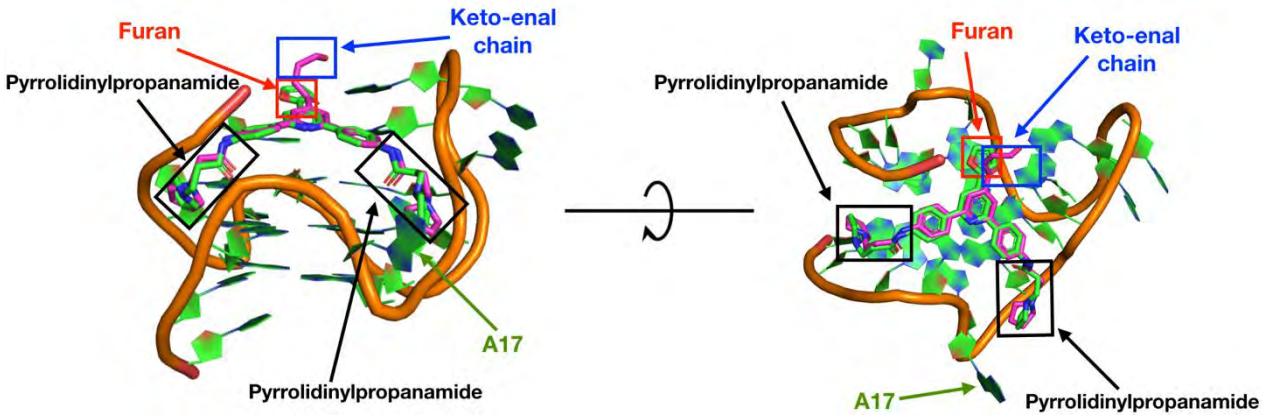

Figure S25. Superimposition of the fifth best docking solution for the furan-closed **TAP-A** (i.e., as obtained with the c-kit conformer #7), with the best docking solution of the oxidized **TAP-A** ligand on the same c-kit conformer.

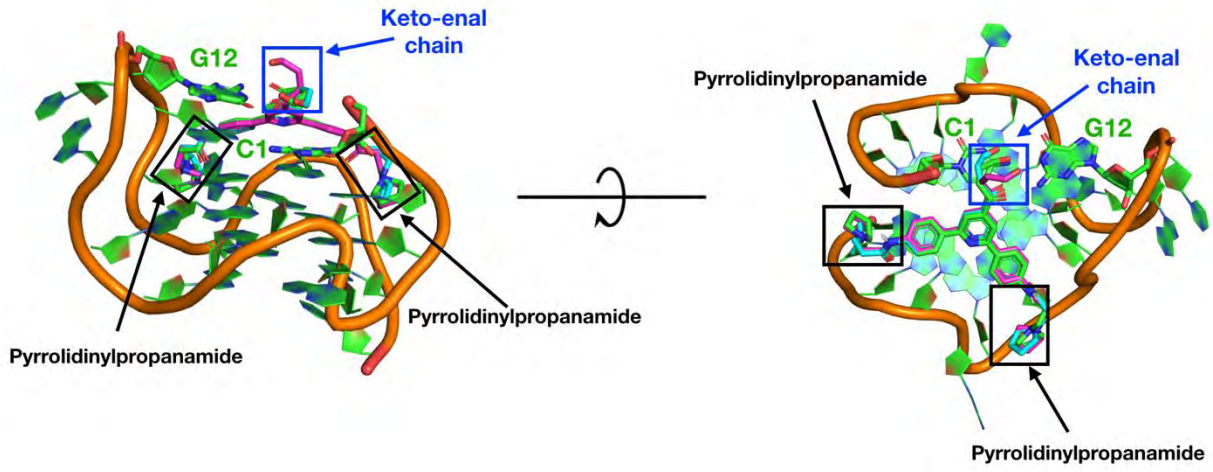

Figure S26. Superimposition of the three best ranked docking solutions for the oxidized **TAP-A**, as obtained with the c-kit conformer #7.

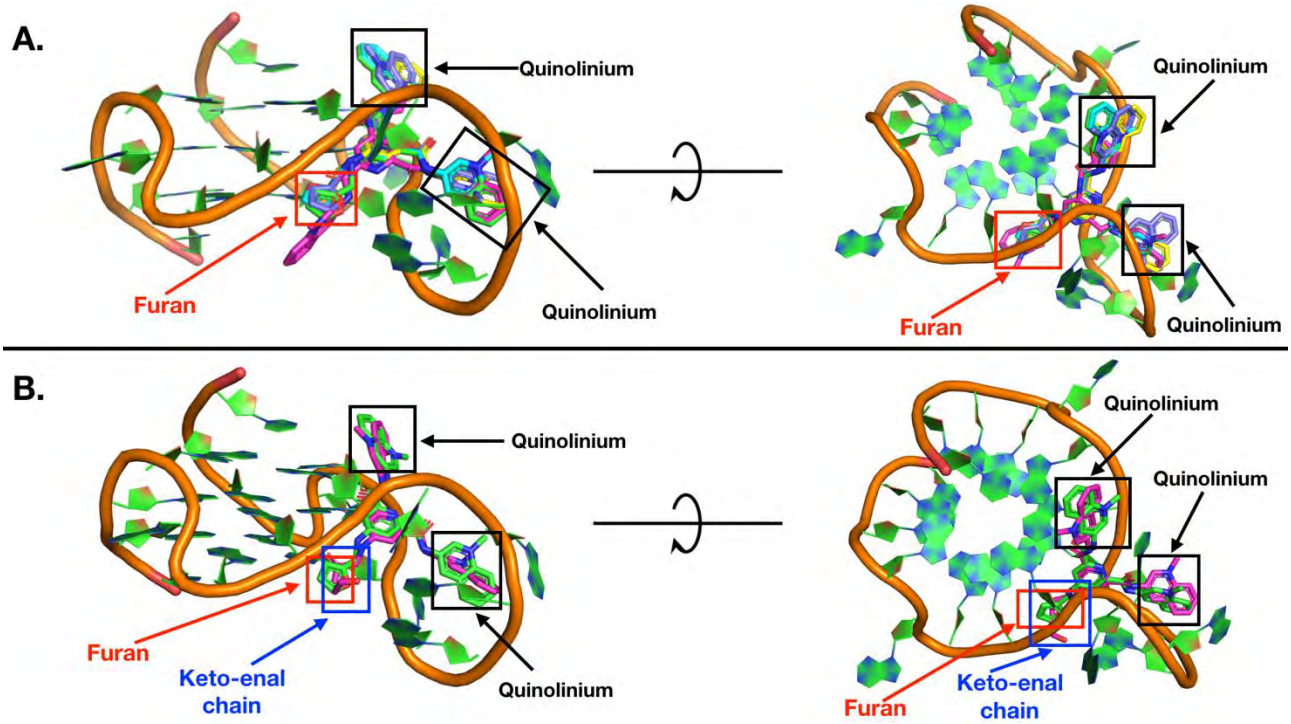

Figure S27. (A) Superimposition of the five best ranked **PDC-A** docking solutions (furan-closed forms of **PDC-A**) as obtained with the c-kit conformer #8 (PDB ID: 2KQH). (B) Superimposition of the best **PDC-A** docking solutions for the furan-closed and oxidized forms of the ligand, as obtained with the c-kit conformer #8 (PDB ID: 2KQH). **PDC-A** is mainly docked in the L2 loop of c-kit. These five solutions are well superposed, except for one docking solution (ranked 5) in which we observed a docking pose in the same c-Kit region but with an exchange between the positioning of quinolinium and furan moieties.

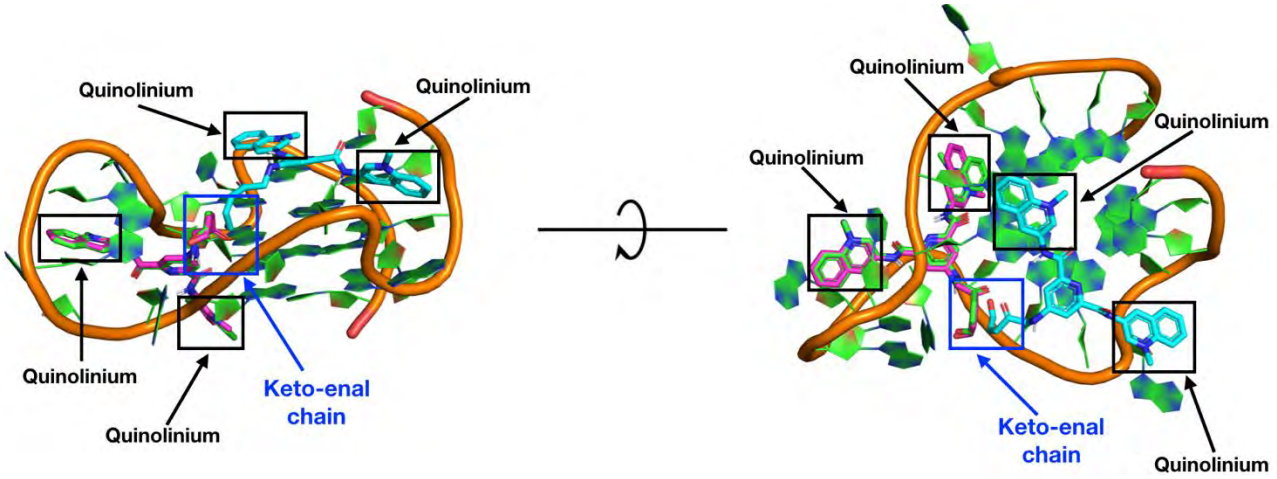

Figure S28. (A) Superimposition of the three best ranked docking solutions for the oxidized **PDC-A**, as obtained with the c-kit conformer #8.

10.3. Supplementary discussion: modelling studies on TAP-B and PDC-B

Among the five best ranked docking solutions of **TAP-B**, one is encountered with conformer #6 of c-kit (ranked 1) and the four others (ranked 2 to 5) with conformer #3 (Figure S29). Docking studies with the furan-opened **TAP-B** show that **TAP-B** oxidation does not strongly impact binding modes: in the case of the c-kit conformer #6, furan and keto-enal are superimposed, whereas **TAP-B** oxidation influences the ligand binding mode for the c-kit conformer #3 (Figure S30). In both cases, the longer keto-enal chain is positioned in such a way that no nitrogen atom from c-kit exocyclic amines was detected close to the reactive carbon atom (with a threshold distance of 4.0 Å). For **PDC-B** ligand, the five best ranked docking solutions are encountered with the c-kit conformer #8 (Figure S29). Again, the furan-opened ligand shows that **PDC-B** oxidation does not influence the docking of the aromatic moieties (Figures S31). Interestingly, superimposition of the three best ranked docking solutions of oxidized **PDC-B** shows different possible positions of the keto-enal group (Figure S32). Despite this flexibility, there are no nitrogen atoms of exocyclic amines close to the reactive carbon in these three docking solutions.

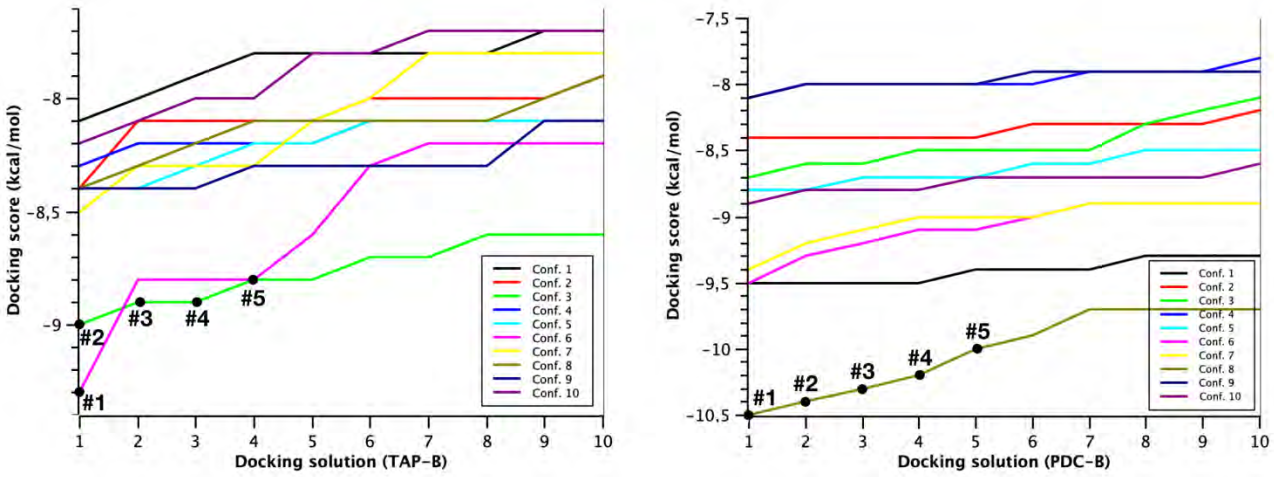

Figure S29. Energy scores of the ten recorded docking solutions for **TAP-B** (left) and **PDC-B** (right) ligands according to each conformer issued from the NMR coordinates of c-kit (PDB ID: 2KQH).

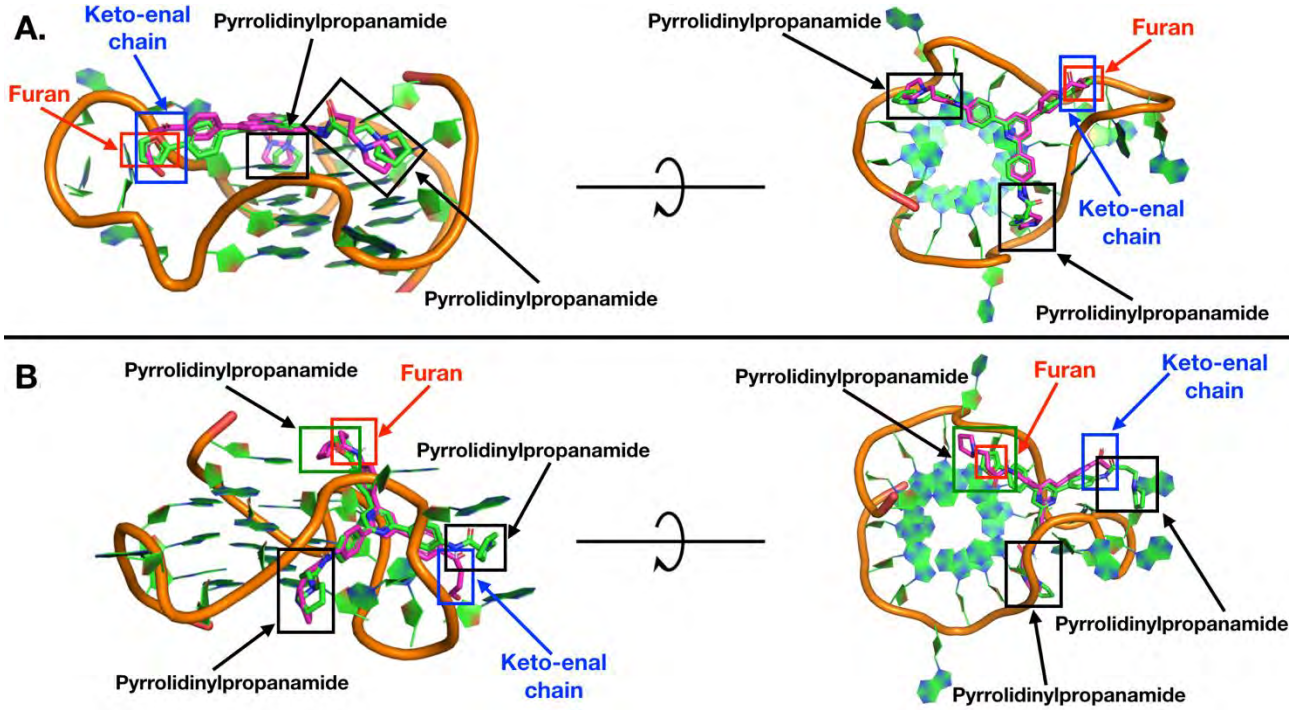

Figure S30. (A) Superimposition of the best ranked **TAP-B** docking solutions for the furan-closed and oxidized forms of the ligand, as obtained with the c-kit conformer #6 (PDB ID: 2KQH). (B) Superimposition of the best ranked **TAP-B** docking solutions for the furan-closed and oxidized forms of the ligand, as obtained with the c-kit conformer #3 (PDB ID: 2KQH).

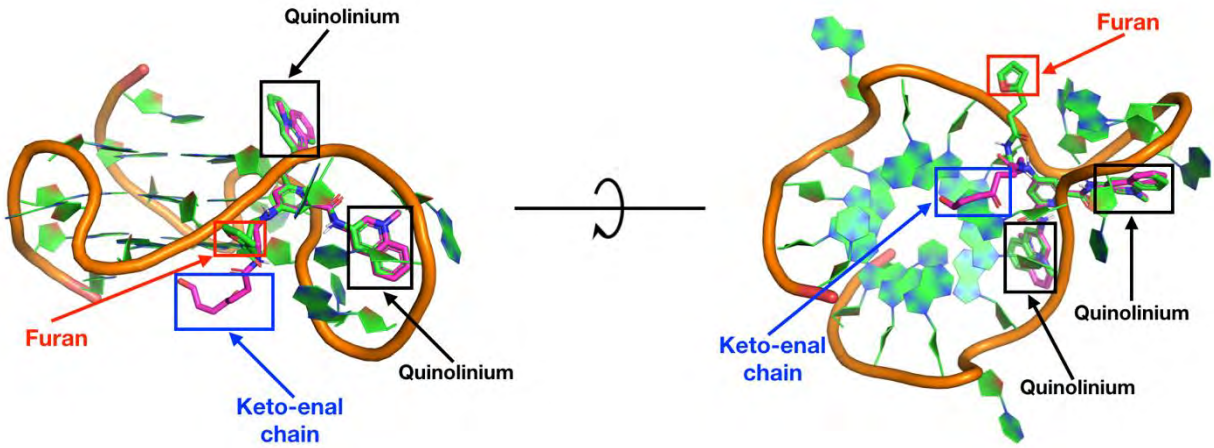

Figure S31. (A) Superimposition of the best ranked **PDC-B** docking solutions for the furan-closed and oxidized forms of the ligand, as obtained with the c-kit conformer #8 (PDB ID: 2KQH).

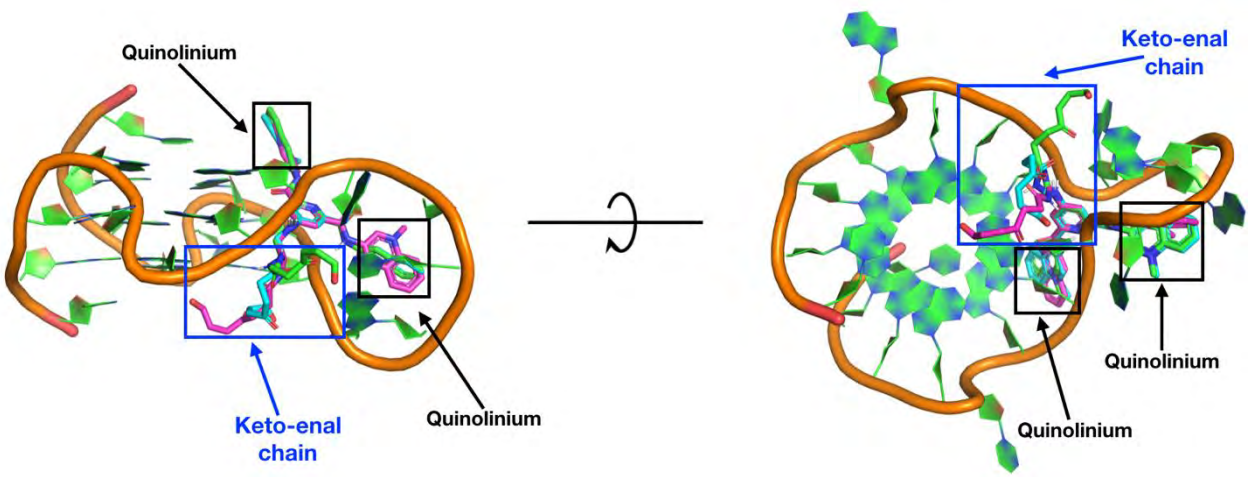

Figure S32. Superimposition of the three best ranked docking solutions for the oxidized **PDC-B**, as obtained with the c-kit conformer #8.

10.4. Supplementary discussion: modelling studies on ligand co-localization

To assess the possibility that MB and one ligand molecule can be co-localized simultaneously around the same G4 target (c-kit), we performed docking calculations of MB alone on the G4 conformers that are related to the 'reactive' binding mode of the four ligands, i.e. conformer #7 for TAP-A, conformer #8 for PDC-A, conformer #3 for TAP-B, conformer #8 for PDC-B. We compared MB and ligand binding modes, giving a clue at the atomistic resolution of the co-localization of MB and synthesized ligands. For TAP-A, the best MB binding mode is superposed with the TAP-A reactive binding mode (Figure S33A). However, affinity scores of the five best ranked docking solutions of MB with G4 conformer #7 are almost identical, *i.e.* with a difference of only 0.4 kcal/mol between ranked #1 and ranked #5 docking solutions (Figure S33B). Three of the top five docking solutions of MB (ranked #2, #3 and #4) are in bottom modes (Figure S33C), indicating that MB could be docked in top mode as well as bottom mode. Additionally, a more stable affinity score is obtained for TAP-A, i.e., -8.8 kcal/ mol versus -6.5 kcal/mol for MB. This means that TAP-A competes with MB in the top binding mode, which forces MB to the bottom binding mode, i.e. interaction with the lower G-tetrad (Figure S33D). For PDC-A, docked in lateral loop L2, the best binding modes of both PDC-A and MB can be conciliated, without any superposition between both MB and PDC-A best binding modes (Figure S33E). Interestingly, as MB is preferentially docked with the lower G-tetrad (for G4 conformer #8), the PDC-A furan moiety is then particularly close to the MB ligand, pointing in its direction. For TAP-B and PDC-B ligands, although best binding modes of both ligands and MB are compatible, i.e., without superposition in the same G4 region (Figure S33F and G), the lack of reactivity of both TAP-B and PDC-B ligands is explained by their docking modes, showing no close extra-cyclic amines, as explained earlier in the main text.

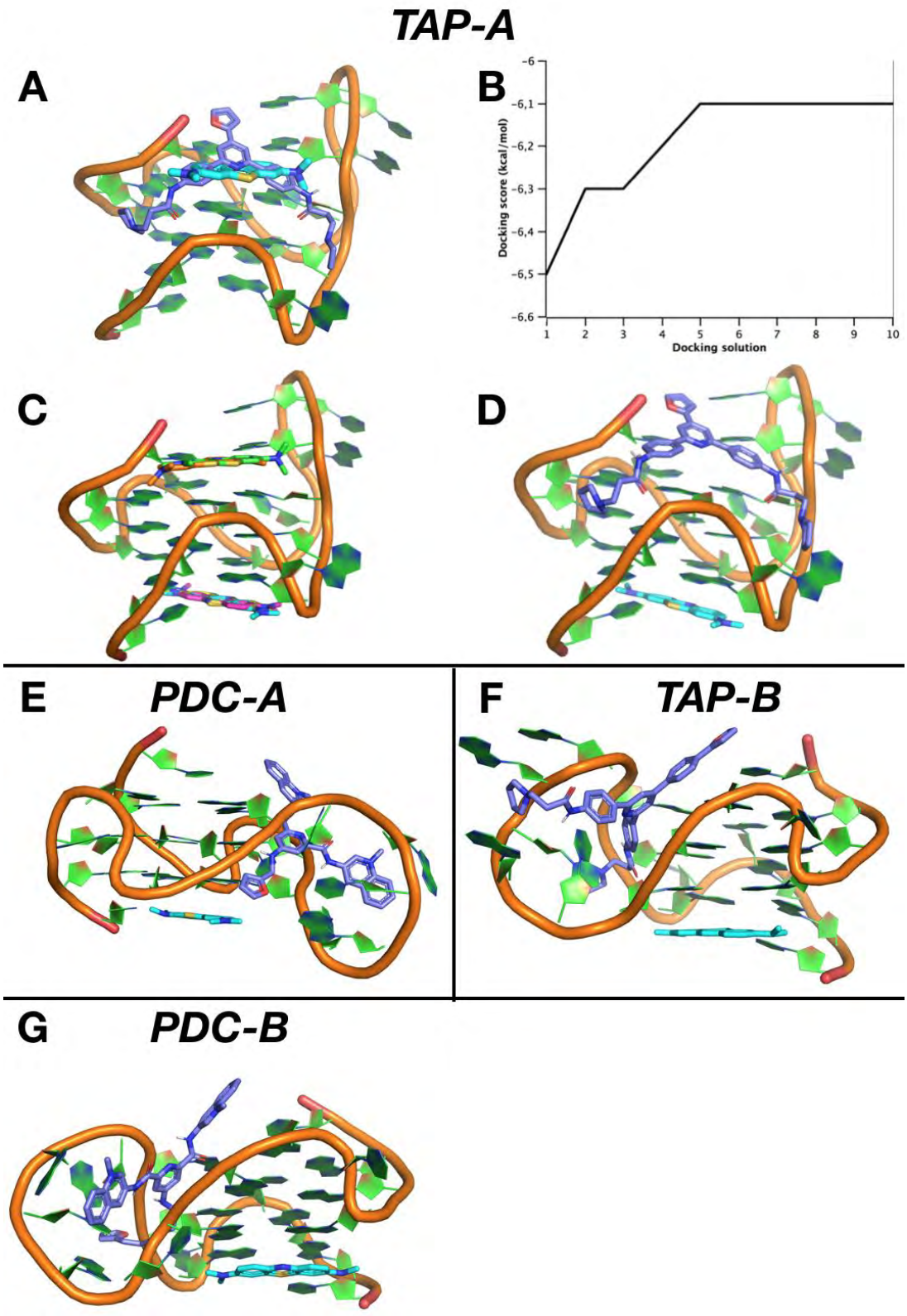

Figure S33. Superimposition of binding modes for each type of ligand (in violet) and methylene blue (in turquoise) on a G4 target conformer of c-kit, showing the possible co-localization of ligands and the preferential adsorption of methylene blue on the lower G-tetrad of c-kit. (A) Superimposition of the best docking solutions of TAP-A and MB with G4 (conformer #8) (B) The scores of the 10 best-ranked solutions of MB on G4. (C) The top five docking solutions of MB with the same G4 (conformer #8) (D) Possible solution for the co-localization of TAP-A and MB on the same G4, see details in the text above. (E) Possible solution for the co-localization of PDC-A/MB on G4 (conformer #8). (F) Possible solution for the co-localization of TAP-B and MB on G4 (conformer #3). (G) Possible solution for the co-localization of PDC-B and MB on G4 (conformer #8).

11. Supporting References

(S1) Smith, N. M.; Labrunie, G.; Corry, B.; Tran, P. L. T.; Norret, M.; Djavaheri-Mergny, M.; Raston, C. L.; Mergny, J. L. Unraveling the Relationship between Structure and Stabilization of Triarylpyridines as G-Quadruplex Binding Ligands. *Org. Biomol. Chem.* **2011**, *9* (17), 6154–6162. https://doi.org/10.1039/c1ob05560g.

(S2) Renaud De La Faverie, A.; Hamon, F.; Di Primo, C.; Largy, E.; Dausse, E.; Delaurire, L.; Landras-Guetta, C.; Toulmé, J. J.; Teulade-Fichou, M. P.; Mergny, J. L. Nucleic Acids Targeted to Drugs: SELEX against a Quadruplex Ligand. *Biochimie* **2011**, *93* (8), 1357–1367. https://doi.org/10.1016/j.biochi.2011.05.022.

(S3) Kuznetsova, N. A.; Gretsova, N. S.; Yuzhakova, O. A.; Negrimovskii, V. M.; Kaliya, O. L.; Luk'yanets, E. A. New Reagents for Determination of the Quantum Efficiency of Singlet Oxygen Generation in Aqueous Media. *Russ. J. Gen. Chem.* **2001**, *71* (1), 36–41. https://doi.org/10.1023/A:1012369120376.

(S4) Cubberley, M. S.; Iverson, B. L. 1 H NMR Investigation of Solvent Effects in Aromatic Stacking Interactions. *J. Am. Chem. Soc.* **2001**, *123* (31), 7560–7563. https://doi.org/10.1021/ja015817m.

(S5) Seidel, C. A. M.; Schulz, A.; Sauer, M. H. M. Nucleobase-Specific Quenching of Fluorescent Dyes. 1. Nucleobase One-Electron Redox Potentials and Their Correlation with Static and Dynamic Quenching Efficiencies. *J. Phys. Chem.* **1996**, *100* (13), 5541–5553. https://doi.org/10.1021/jp951507c.

(S6) Nordén, B.; Tjerneld, F. Structure of Methylene Blue-DNA Complexes Studied by Linear and Circular Dichroism Spectroscopy. *Biopolymers* **1982**, *21* (9), 1713–1734. https://doi.org/10.1002/bip.360210904.

(S7) Zhang, F. T.; Nie, J.; Zhang, D. W.; Chen, J. T.; Zhou, Y. L.; Zhang, X. X. Methylene Blue as a G-Quadruplex Binding Probe for Label-Free Homogeneous Electrochemical Biosensing. *Anal. Chem.* **2014**, *86* (19), 9489–9495. https://doi.org/10.1021/ac502540m.

(S8) Epe, B.; Pflaum, M.; Boiteux, S. DNA Damage Induced by Photosensitizers in Cellular and Cell-Free Systems. *Mutat. Res. Toxicol.* **1993**, *299* (3–4), 135–145. https://doi.org/10.1016/0165-1218(93)90091-Q.

(S9) OhUigin, C.; McConnell, D. J.; Kelly, J. M.; van der Putten, W. J. M. Methylene Blue Photosensitised Strand Cleavage of DNA: Effects of Dye Binding and Oxygen. *Nucleic Acids Res.* **1987**, *15* (18), 7411–7427. https://doi.org/10.1093/nar/15.18.7411.

(S10) Hanwell, M. D.; Curtis, D. E.; Lonie, D. C.; Vandermeerschd, T.; Zurek, E.; Hutchison, G. R. Avogadro: An Advanced Semantic Chemical Editor, Visualization, and Analysis Platform. *J. Cheminform.* **2012**, *4* (8). https://doi.org/10.1186/1758-2946-4-17.

(S11) Wang, J.; Wolf, R. M.; Caldwell, J. W.; Kollman, P. A.; Case, D. A. Development and Testing of a General Amber Force Field. *J. Comput. Chem.* **2004**, *25* (9), 1157–1174. https://doi.org/10.1002/jcc.20035.

(S12) Hassan, N. M.; Alhossary, A. A.; Mu, Y.; Kwoh, C. K. Protein-Ligand Blind Docking Using QuickVina-W with Inter-Process Spatio-Temporal Integration. *Sci. Rep.* **2017**, *7* (1), 1–13. https://doi.org/10.1038/s41598-017-15571-7.

(S13) Jaghoori, M. M.; Bleijlevens, B.; Olabarriaga, S. D. 1001 Ways to Run AutoDock Vina for Virtual Screening. *J. Comput. Aided. Mol. Des.* **2016**, *30* (3), 237–249. https://doi.org/10.1007/s10822-016-9900-9.

(S14) Delano, W. L. **(2002)**. *The PyMOL Molecular Graphics System*. Available online at: https://ci.nii.ac.jp/naid/10020095229/en/

12. Characterizations

12.1. NMR spectra

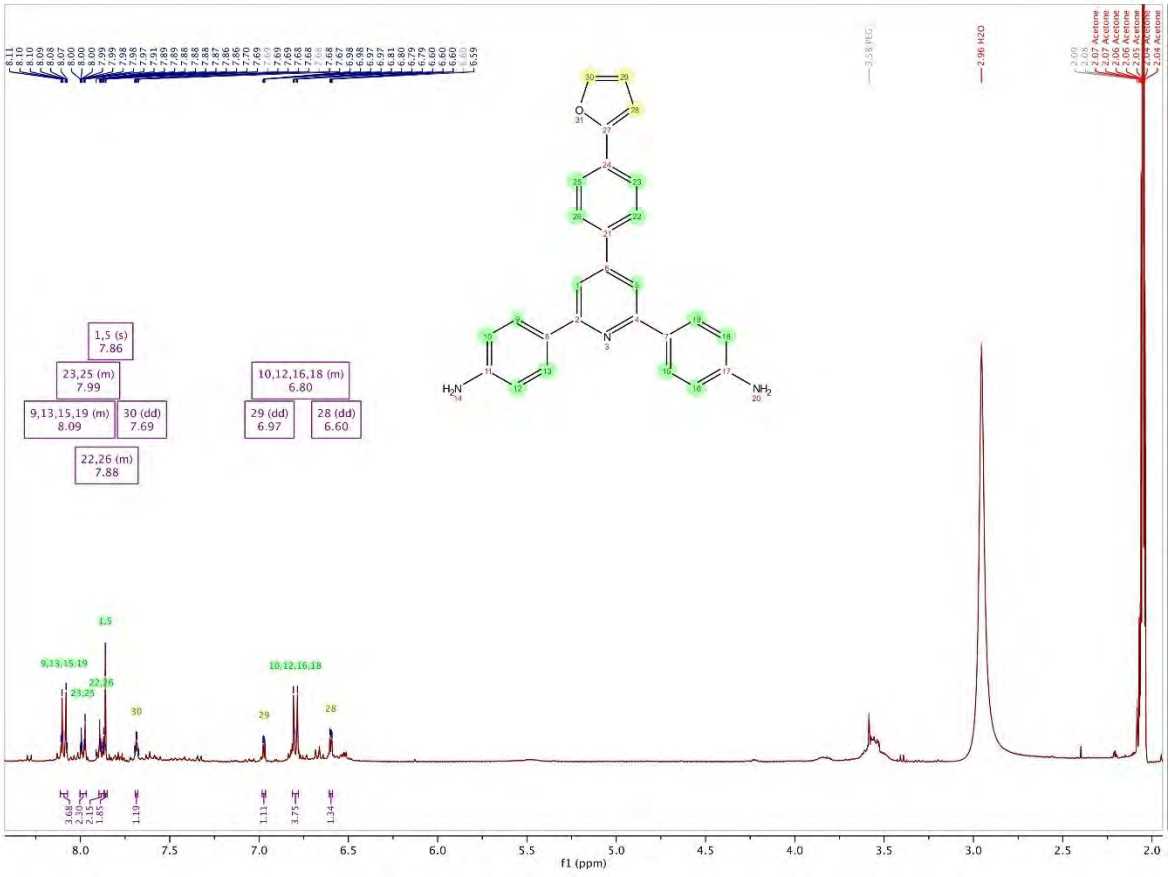

Figure S34. ^{1}H-NMR of compound **S2-b**

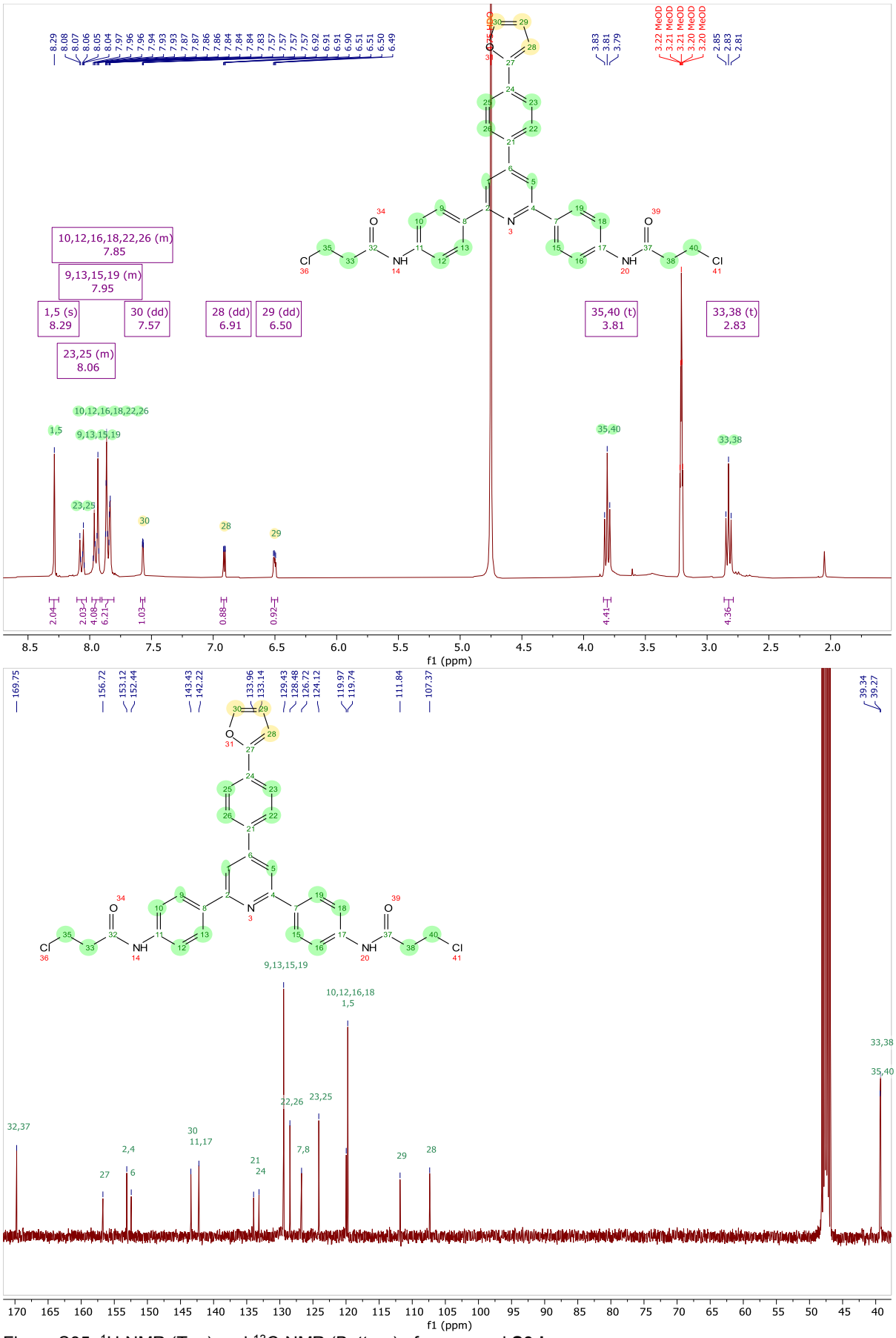

Figure S35. ^{1}H-NMR (Top) and ^{13}C-NMR (Bottom) of compound **S3-b**.

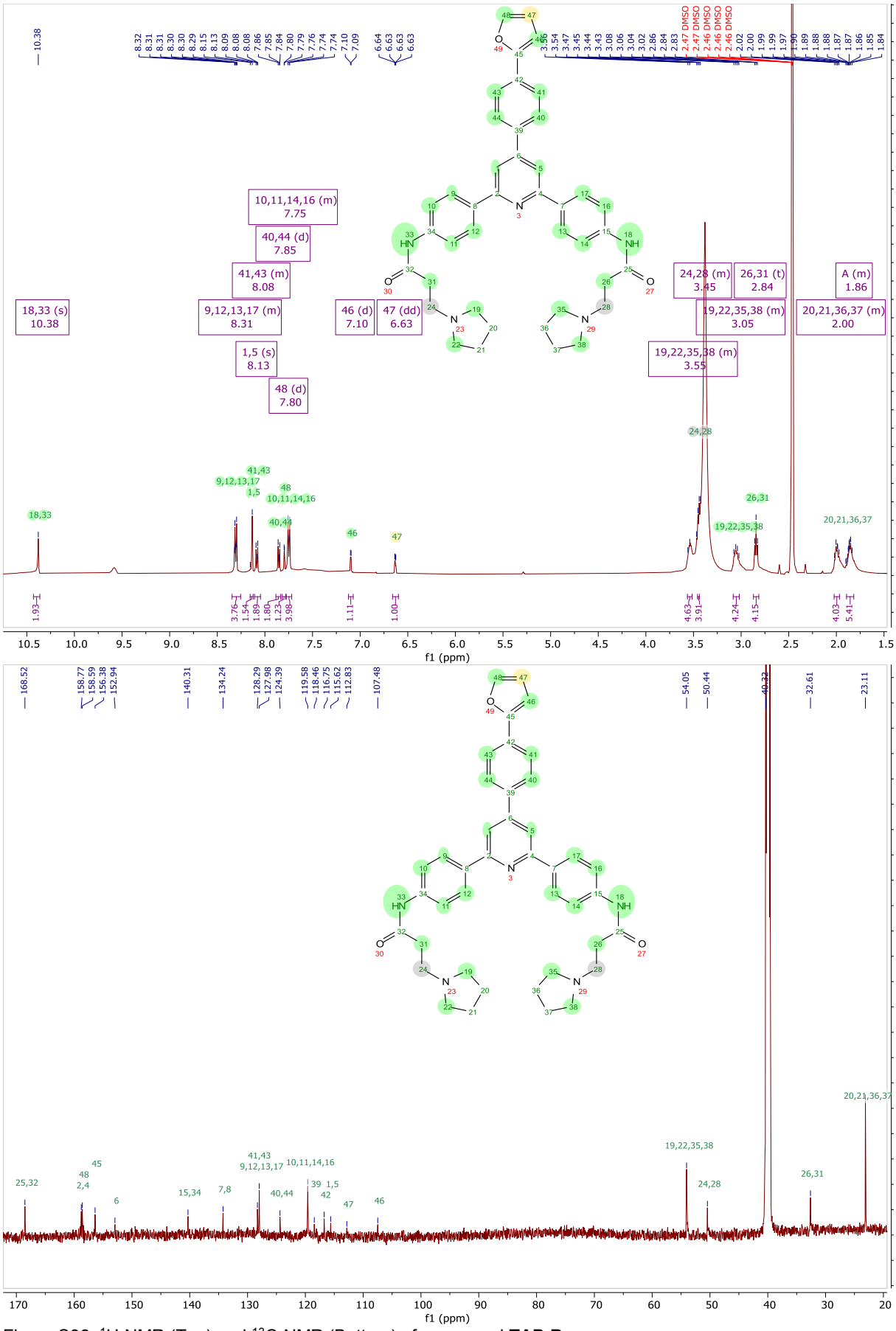

Figure S36. ^{1}H-NMR (Top) and ^{13}C-NMR (Bottom) of compound **TAP-B.**

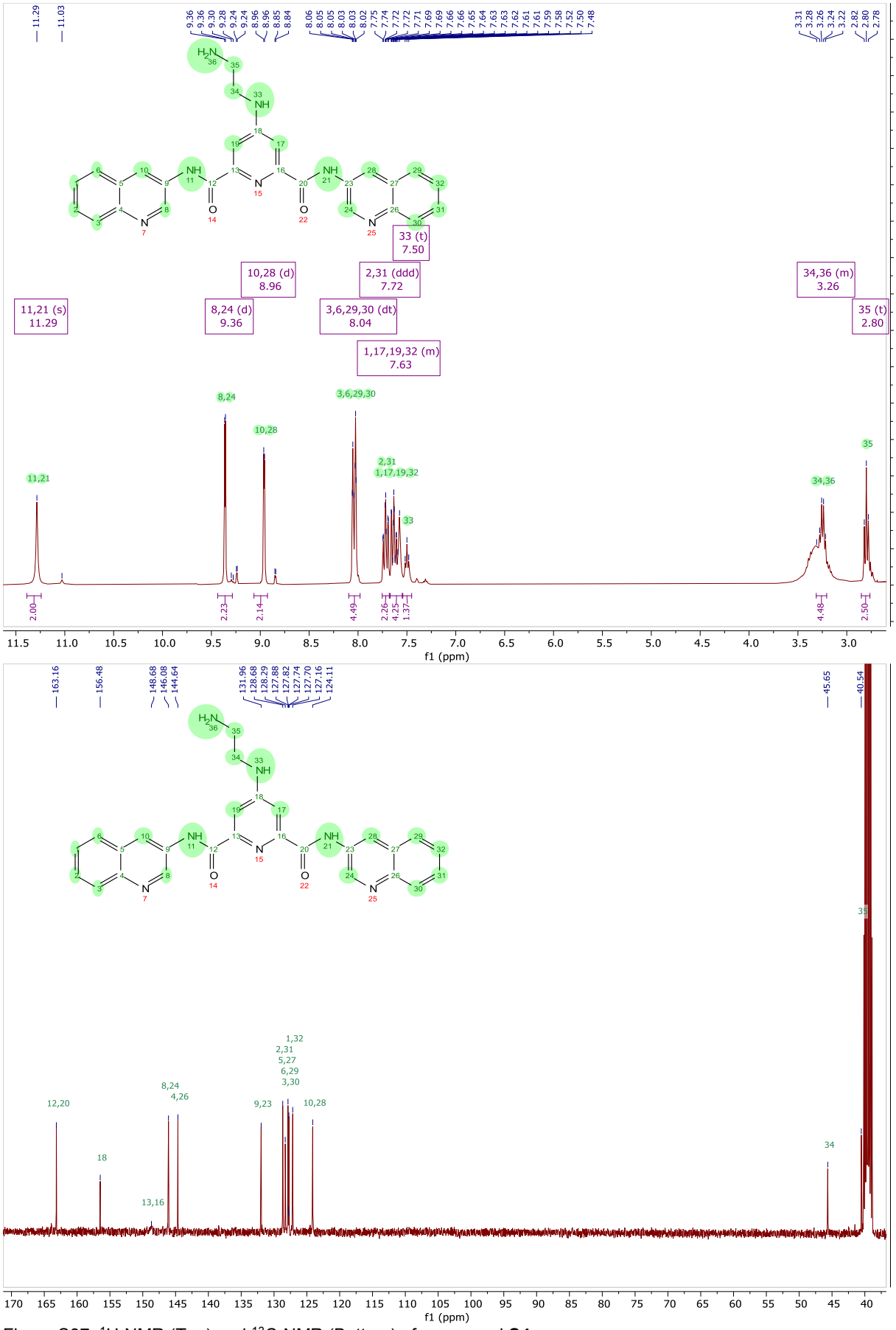

Figure S37. ^{1}H-NMR (Top) and ^{13}C-NMR (Bottom) of compound **S4**.

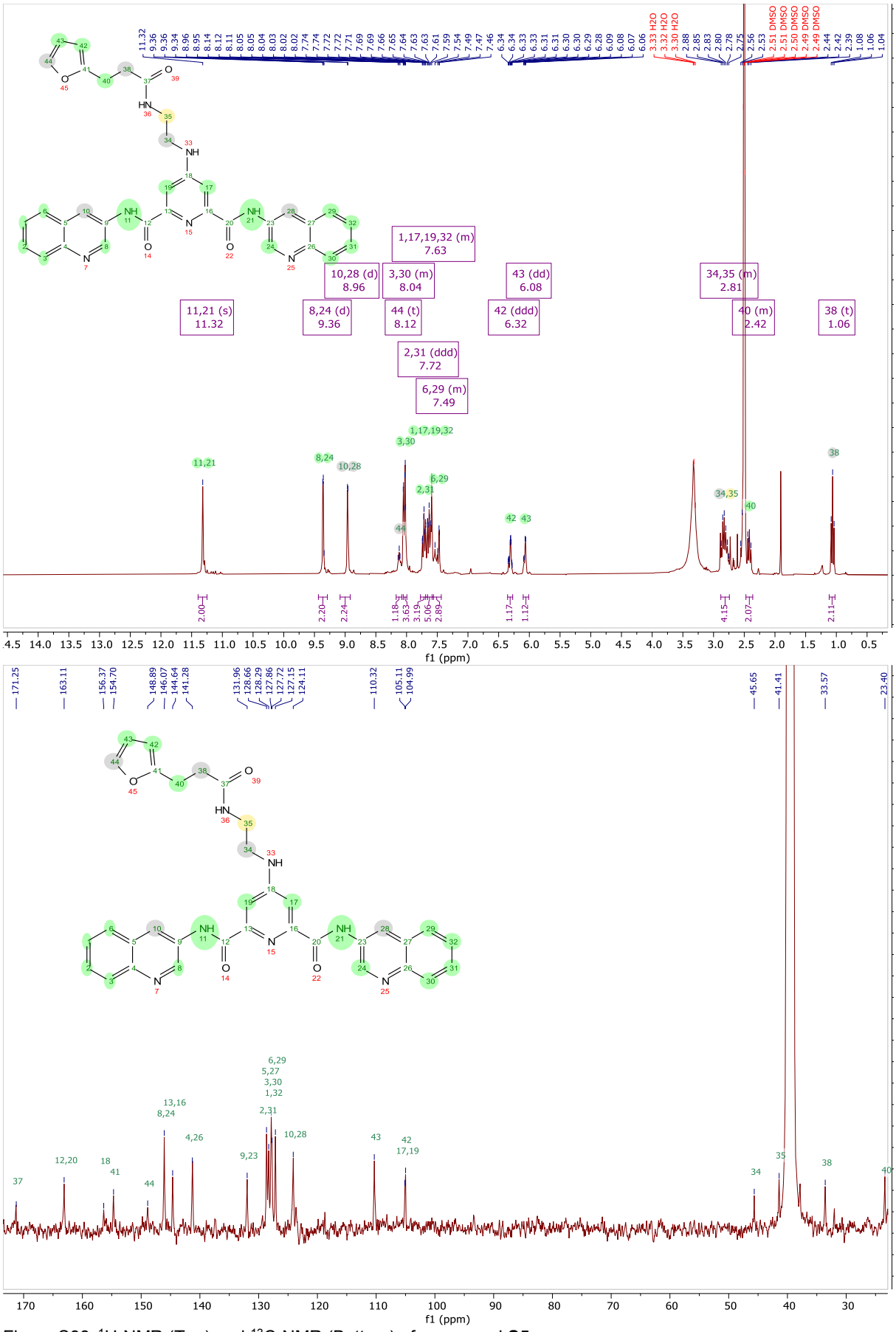

Figure S38. ^{1}H-NMR (Top) and ^{13}C-NMR (Bottom) of compound **S5.**

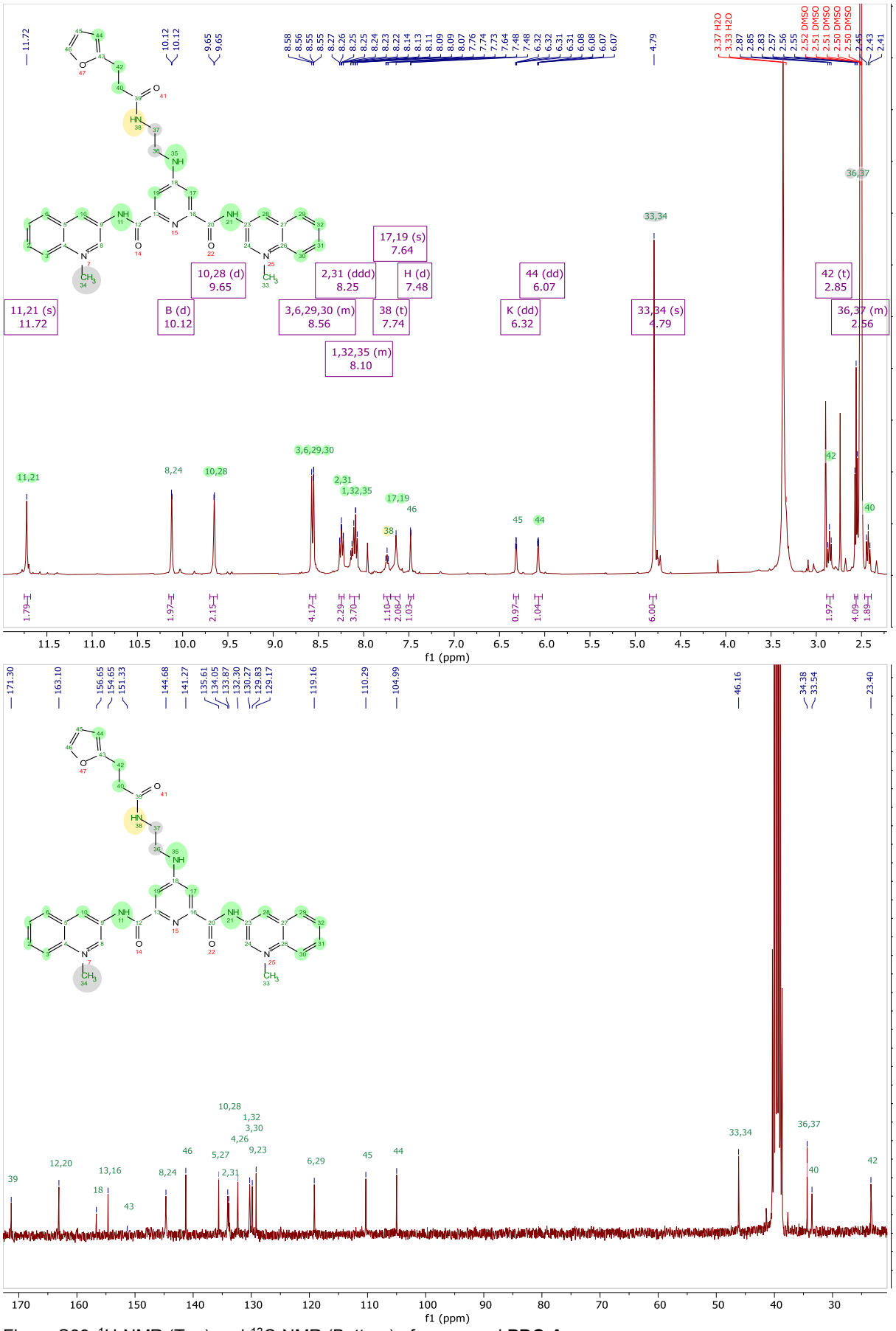

Figure S39. ^{1}H-NMR (Top) and ^{13}C-NMR (Bottom) of compound **PDC-A**.

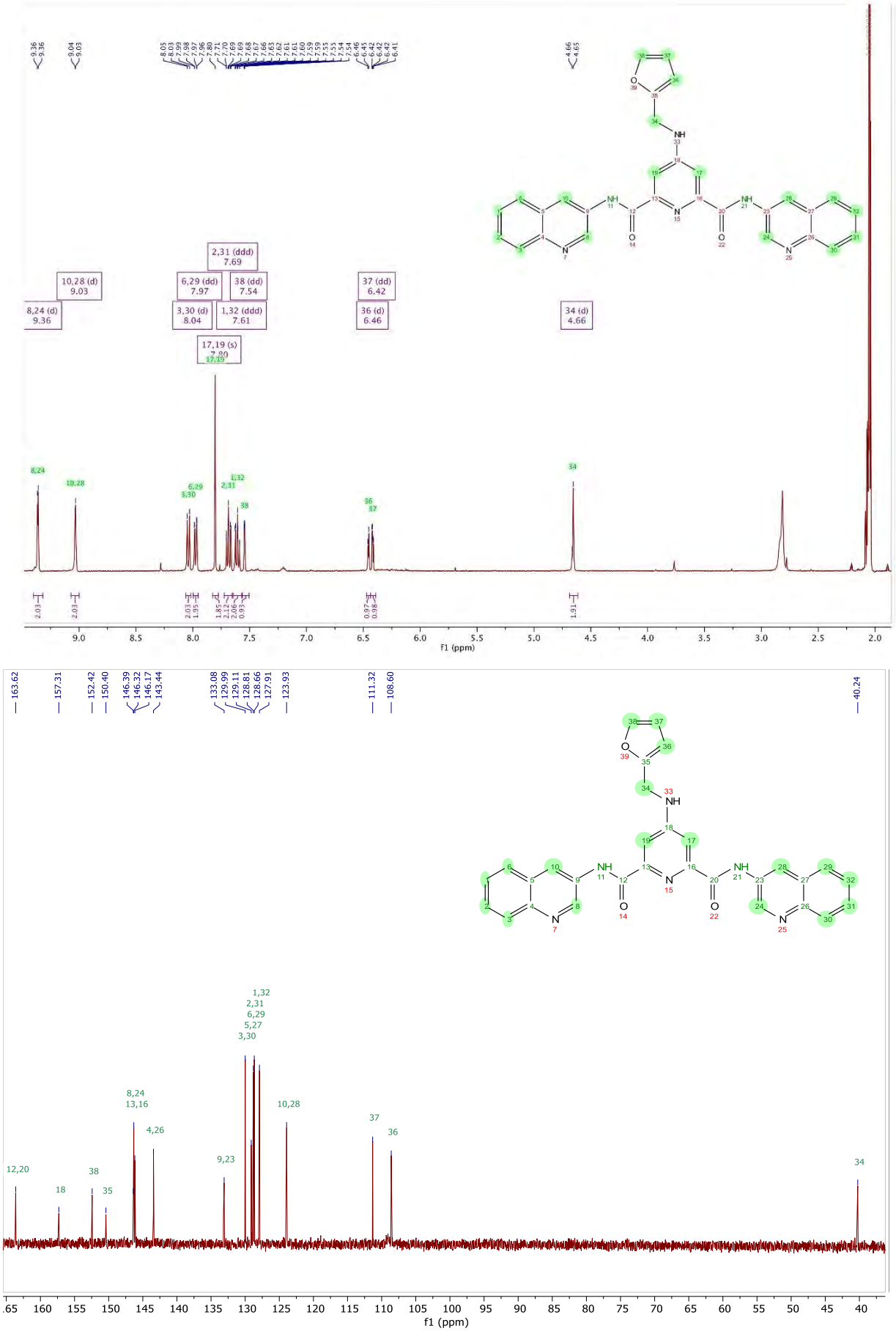

Figure S40. ^{1}H-NMR (Top) and ^{13}C-NMR (Bottom) of compound **S6**.

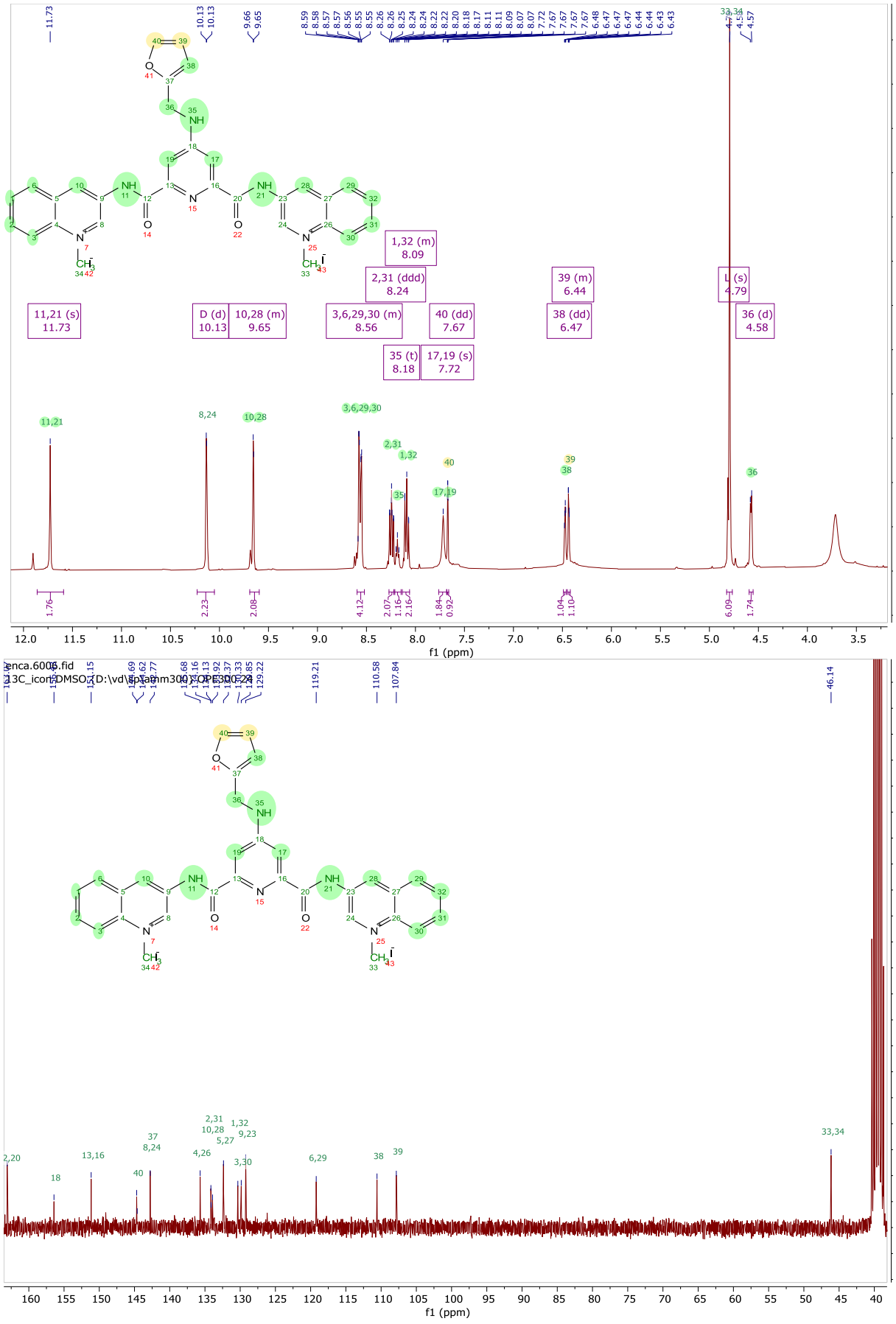

Figure S41. ^{1}H-NMR (Top) and ^{13}C-NMR (Bottom) of compound **PDC-B**